AD-A186 956 SUPERLATTICE PHOTODETECTORS(U) ROCKWELL INTERNATIONAL 1/1
THOUSAND OAKS CA MICROELECTRONICS RESEARCH AND DEVELO
PMENT CENTER S W ZEHR AUG 87 MRDC41140.10FR
UNCLASSIFIED RADC-TR-87-102 F19628-83-C-0055 F/G 17/5 NL

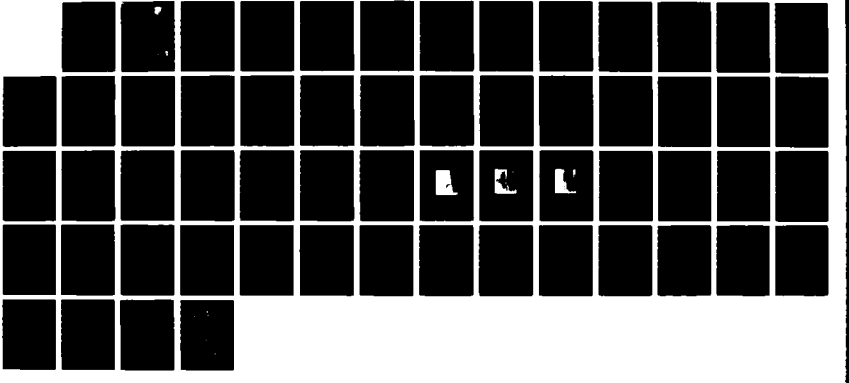

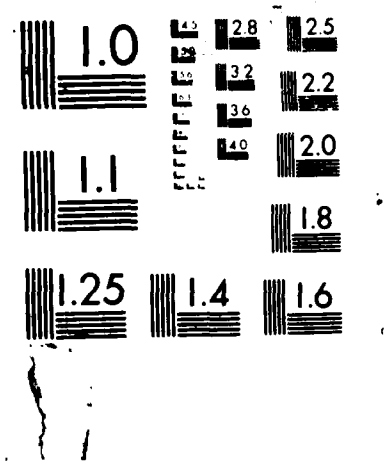
1.0
1.1
1.25
1.4
1.6
1.8
2.0
2.2
2.5
2.8
3.2
3.6
4.0

RADC-TR-87-102
Final Technical Report
August 1987

SUPERLATTICE PHOTODETECTORS

Rockwell International/MRDC

Stanley W. Zehr

ROME AIR DEVELOPMENT CENTER
Air Force Systems Command
Griffiss Air Force Base, NY 13441-5700

This report has been reviewed by the RADC Public Affairs Office (PA) and is releasable to the National Technical Information Service (NTIS). At NTIS it will be releasable to the general public, including foreign nations.

RADC-TR-87-102 has been reviewed and is approved for publication.

APPROVED: Thomas G. Ryan

THOMAS G. RYAN
Project Engineer

APPROVED: Harold Roth

HAROLD ROTH
Director of Solid State Sciences

FOR THE COMMANDER: John A. Ritz

JOHN A. RITZ
Directorate of Plans & Programs

If your address has changed or if you wish to be removed from the RADC mailing list, or if the addressee is no longer employed by your organization, please notify RADC (ESOC) Hanscom AFB MA 01731-5000. This will assist us in maintaining a current mailing list.

Do not return copies of this report unless contractual obligations or notices on a specific document require that it be returned.

UNCLASSIFIED
SECURITY CLASSIFICATION OF THIS PAGE

ADA186956

REPORT DOCUMENTATION PAGE

Form Approved
OMB No 0704-0188

1a REPORT SECURITY CLASSIFICATION UNCLASSIFIED	1b RESTRICTIVE MARKINGS N/A
2a SECURITY CLASSIFICATION AUTHORITY N/A	3 DISTRIBUTION/AVAILABILITY OF REPORT Approved for public release; distribution unlimited
2b DECLASSIFICATION/DOWNGRADING SCHEDULE N/A	
4 PERFORMING ORGANIZATION REPORT NUMBER(S) MRDC41140.10FR	5 MONITORING ORGANIZATION REPORT NUMBER(S) RADC-TR-87-102
6a NAME OF PERFORMING ORGANIZATION Rockwell International/MRDC 6b OFFICE SYMBOL (If applicable)	7a NAME OF MONITORING ORGANIZATION Rome Air Development Center (ESOC)
6c ADDRESS (City, State, and ZIP Code) Microelectronics Research and Development Center 1049 Camino Dos Rios Thousand Oaks CA 91362	7b ADDRESS (City, State, and ZIP Code) Hanscom AFB MA 01731-5000
8a NAME OF FUNDING/SPONSORING ORGANIZATION Rome Air Development Center 8b OFFICE SYMBOL (If applicable) ESOC	9 PROCUREMENT INSTRUMENT IDENTIFICATION NUMBER F19628-83-C-0055
8c ADDRESS (City, State, and ZIP Code) Hanscom AFB MA 01731-5000	10 SOURCE OF FUNDING NUMBERS PROGRAM ELEMENT NO: 63220C; PROJECT NO: 2306; TASK NO: J2; WORK UNIT ACCESSION NO: 48

11 TITLE (Include Security Classification)
SUPERLATTICE PHOTODETECTORS

12 PERSONAL AUTHOR(S)
Stanley W. Zehr

13a TYPE OF REPORT	13b TIME COVERED	14 DATE OF REPORT (Year, Month, Day)	15 PAGE COUNT
Final	FROM Jul 83 TO May 85	August 1987	60

16 SUPPLEMENTARY NOTATION
N/A

17 COSATI CODES			18 SUBJECT TERMS (Continue on reverse if necessary and identify by block number)
FIELD	GROUP	SUB-GROUP	low noise, avalanche, high sensitivity, photodiodes, superlattice
17	02		
20	06		

19 ABSTRACT (Continue on reverse if necessary and identify by block number)

The technical progress in Phase 1 of this two-phase program aimed at development of low noise high sensitivity superlattice avalanche photodiodes is reported. The initial focus of the Phase 1 effort was development of metalorganic chemical vapor deposition (MOCVD) technology for the growth of high quality GaAs/AlGaAs superlattice structures. Using the developed growth technology, two series of GaAs/AlGaAs structures were evaluated with regard to dark current, breakdown voltage, and dark and illuminated gain characteristics to study effects of variations in critical growth and structural parameters. The results will be used to guide development of a predictive performance model for this class of devices during Phase 2 of the program. The model will then be applied to optimizing design of low noise, high sensitivity InGaAs/InP APD's operating in the low loss 1.0 to 1.6μmwavelength range. Such devices will be grown by MOCVD and their performance evaluated during Phase 2 of the program.

20 DISTRIBUTION/AVAILABILITY OF ABSTRACT	21 ABSTRACT SECURITY CLASSIFICATION	
☐ UNCLASSIFIED/UNLIMITED ☐ SAME AS RPT ☒ DTIC USERS	UNCLASSIFIED	
22a NAME OF RESPONSIBLE INDIVIDUAL Thomas C. Ryan	22b TELEPHONE (Include Area Code) (617) 377-4925	22c OFFICE SYMBOL RADC (ESOC)

DD Form 1473, JUN 86 — Previous editions are obsolete — SECURITY CLASSIFICATION OF THIS PAGE

UNCLASSIFIED

1.0 INTRODUCTION

1.1 Program Outline

The aim of this program is to develop improved low noise avalanche photodiodes (APD's) operating in the 1.3 to 1.55 μm wavelength range. This is to be done by manipulating the ratio of electron to hole ionization rates (α/β) through the use of multilayered structures in the avalanche region of the devices. The program is divided into two major phases. In the first phase, the influence of structural device parameters on ionization processes in AlGaAs/GaAs structures grown by MOCVD were examined both theoretically and experimentally. In the second phase, experimental avalanche structures responding in the 1.3 to 1.55 μm wavelength range are to be fabricated from MOCVD-grown InP/InGaAs layers. The effects of structural device parameters upon the ionization processes in these devices will be evaluated. In parallel with the experimental activities, a theoretical modeling effort will be carried out to develop a coherent framework to interpret the experimental results and guide device optimization.

Following the Background section immediately below, activities and progress during phase I of the program are described. Plans for the phase II effort are then discussed.

1.2 Background

The application of high sensitivity, high data rate, multichannel video and voice optical communication systems for Air Force systems programs requires the availability of low noise, very high speed avalanche photodiodes APD's. For

repeaterless long distance communications networks, the photodetectors must operate in the 1.3 to 1.6 μm wavelength range where the loss in commercially available optical fibers is less than 2 dB/km. These requirements are not effectively met by conventional avalanche photodiodes.

Currently available APD's which operate in this wavelength range are made from III-V compound semiconductors which have electron (α) and hole (β) ionization coefficients which are nearly equal. As a result, large excess noise factors and pulse broadening occur in these devices even at moderate gains (~ 5). At higher gains, these effects can lead to substantial system degradation. It is desirable to alter the α/β ratio from its value near 1 to minimize these effects. The α/β ratio has traditionally been considered to be a fixed property for a given material. Attempts to alter this ratio significantly through variations of the composition of bulk materials have not been successful.

An alternative approach by which this ratio might be significantly altered is the incorporation of multiple heterojunctions between ultra thin layers of dissimilar semiconductor materials. This type of superlattice structure was first proposed by Chin et al,[1] and was theoretically pridicted to have an α/β ratio significantly modified from its value in either homogeneous bulk material. The proposed structure was later fabricated in the GaAs/AlGaAs system and qualitatively substantiated the theoretical result[2]. For the first time, the α/β ratio had been modifed through the use of an artificial heterostructure.

Although such structures are relatively complicated as compared to traditional p-n junction photodiodes, recent advances in epitaxial growth technology make them attractive for devices which efficiently respond to wavelengths in the low fiber loss range between 1.0 and 1.6 μm.

1.3 Conventional Avalanche Photodetectors

In the wavelength region 0.7 to 0.9 μm, commercial silicon avalanche photodiodes offer low excess noise, high sensitivity, and good quantum efficiency, but operate at only moderate data rates. High quantum efficiency AlGaAs/GaAs APD's operate in the same wavelength range at data rates in excess of 1 GHz. However, these latter devices exhibit large excess noise factors owing to the near-unity ratio of the ionization coefficients. For the longer wavelength of 1.0 to 1.6 μm, InGaAs photodetectors offer high quantum efficiency and operate at data rates in excess of 1 GHz. Unfortunately, conventional APD's photodiodes fabricated from this material also exhibit large excess noise factors. Typical characteristics of Si, AlGaAs/GaAs and InGaAsP/InP detectors are summarized in Table 1.1.

Table 1.1

Typical Photodiode Operating Characteristics for Fiber-Optic Systems

Type of Avalanche Photodiode	Wavelength of Operation (μm)	Dark Current	Quantum Efficiency	Data Rate	α/β
Silicon	0.7 - 0.9	< 5 nA	70%	< 1 Gbit	> 20
AlGaAs/GaAs	0.7 - 0.9	< 5 nA	95%	> 1 Gbit	~ 1
InGaAsP/InP	1.3 - 1.6	< 10 nA	95%	> 1 Gbit	~ 1 - 4

1.3.1 Effect of Excess Noise Upon Receiver Performance

The ratio of the ionization coefficients affect both the sensitivity and the gain-bandwidth product of an APD. If the ratio is near unity and the data rate is high, the resulting pulse broadening can lead to the smearing of pulses and the loss of information. This temporal smearing limits the ultimate speed at which the detector can operate. In addition, the randomness of the ionization process necessarily introduces excess noise. The result is a reduction in the sensitivity of the detector. The amount of reduction in the signal-to-noise-ratio can be expressed by:

$$\frac{S}{N} = \frac{1/2(q\eta P_o/h\nu)}{2q[(I_p F_p + I_B F_B + I_{DB} F_{DB})B] + [2qI_{DS}B/M^2(\lambda,\omega) + 4kT_{eff}B/R_{eq}M(\lambda,\omega)^2]}$$

where

- B: System Bandwidth
- q: Electronic Charge
- η: Quantum Efficiency
- P_o: Average Optical Signal Power
- h: Photon Energy
- M(.): Multiplication Factor
- I_{DB}: Current Due to Background Radiation
- I_B: Dark Current Due to Bulk Leakage
- I_p: Photocurrent
- I_{DS}: Dark Current Due to Surface Leakage
- F_{DB}: Excess Noise Due to Bulk Leakage Multiplication
- F_B: Excess Noise Due to Background Radiation Current Multiplication
- F_p: Excess Noise Due to Photoinduced Current Multiplication

$\frac{4kT_{eff}}{R_{eg}}$: Thermal Noise Current

Avalanche gain can increase the signal-to-noise ratio by decreasing the importance of the last two terms in the denominator. However, the excess noise, F from the avalanche process is always equal to or greater than unity and increases monotonically with multiplication. Thus, there is some optimum value of multiplication which will produce the maximum signal-to-noise ratio for a given optical power. Obviously, decreasing F results in high S/N ratios at any given M.

The shot-noise spectral density for ideal (noise free) multiplication is given by $2\alpha I_t M$. F, the excess noise factor, is defined as:

Actual Shot Noise = F * Ideal Shot Noise

Thus, the actual shot noise is $2\alpha I_t M$ F. In turn, the excess noise factor is directly related to the ratio of ionization coefficients. If we define this ratio as k($k = \alpha/\beta$), we have for electron injection into the high field region

$$F_n = M_n \{1 - (1 - k)[(M_n - 1)/M_2]^2\}$$

For holes injected from the opposite end (spacially) of the device we have

$$F_p = M_p \{1 - [1 - (1/k)][(M_p - 1)/M_p]^2\}$$

Owing to the symmetry in n, p, k, and 1/k, only one set of curves is necessary to show the relation between the excess noise factors and k as a function of multiplication. Such curves are shown in Figure 1. As is evident, the ratio

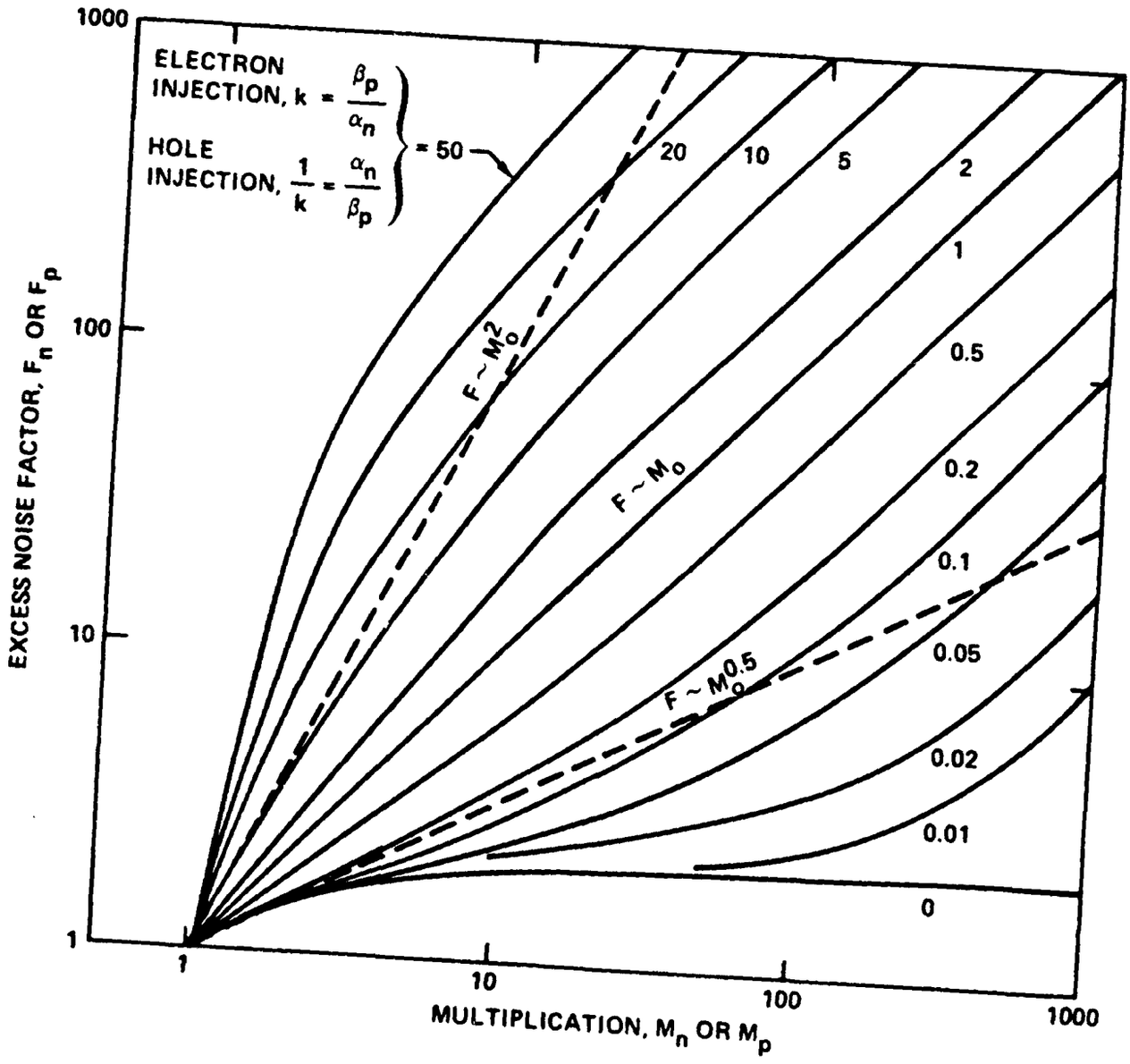

Fig. 1 Excess-noise factors for various values of multiplication and ratios of the electron and hole ionization coefficients.

of the ionization coefficients must be substantially different from unity to obtain low excess noise factors. The noise level varies linearly with the excess noise factor. The effect can be substantial, for example, at gains = 100, a comparison between the case of $\alpha = \beta$ and $\alpha = .01\beta$ shows more than a 9 dB improvement in the signal-to-noise ratio for $\alpha = .01\beta$. This same substantial effect is seen in pulse code modulation (PCM). Shown in Table 1.2 is the effect of the α/β ratio upon the minimum number of primary electrons required to obtain a 10^{-10} bit error rate (BER).

As for the pulse broadening occurring at multiplication values above unity, Anderson et al[4] have shown for average values of multiplication, M, such that

$$(\beta/\alpha)(M_n - 1)\ln(M_n) \leq 1$$

the multiplication is essential independent of frequency. The bandwidth and response time are limited simply by the transit time which is the same as for a nonavalanche PIN detector. Emmons[5] has calculated $F(\omega)$, the normalized frequency response as a function of normalized frequency ωt, where $t = \omega/v_n = \omega/v_p$ ($v_{n,p}$ is the saturated electron and hole velocity, respectively), for the various values of α/β and M. The results of this calculation are shown in Figure 2. The equation $(\beta_p/\alpha_n)(M - 1)\ln(M) = 1$ is shown in the upper portion of the figure. For $\beta_p = \alpha_n$, the onset of pulse broadening occurs at a multiplication value > 7. At a multiplication value of 30, β_p/α_n ratios of 100 or higher are necessary to prevent the onset of pulse broadening. Finally, an analysis by Chang[6] showed that the location of photon absorption had no effect

Table 1.2

Comparison of Minimum Number of Primary Electrons n_{min} Required from an "On" Pulse of a PCM Optical Communications System to Give a 10^{-10} Bit Error Rate[a]

		Ideal Detector (F=1) Poisson Dist.	Ideal Detector (F=1) Eq. (64)	Avalanche Photodiode k=0	Avalanche Photodiode k=0.02	Avalanche Photodiode k=1
(a)	$M=2\times10^4$					
	n_{min}	46	49	115	328	1820
	M_{opt}	large	-	550	150	25
	F_e	1	1	2	5.0	25
	n_{min}/F_e	46	49	57	65	73
(b)	$M=4\times10^3$					
	n_{min}	46	49	115	198	793
	M_{opt}	large	-	110	54	11.0
	F_e	1	1	2	3.0	11.0
	n_{min}/F_e	46	49	57	66	72

[a]Modulation depth is 99% for two different threshold settings of M electrons: (a) $M=2\times10^4$ electrons; (b) $M=4\times10^3$ electrons. The minimum value of m depends on the amplifier noise. (After Webb, et al).[3]

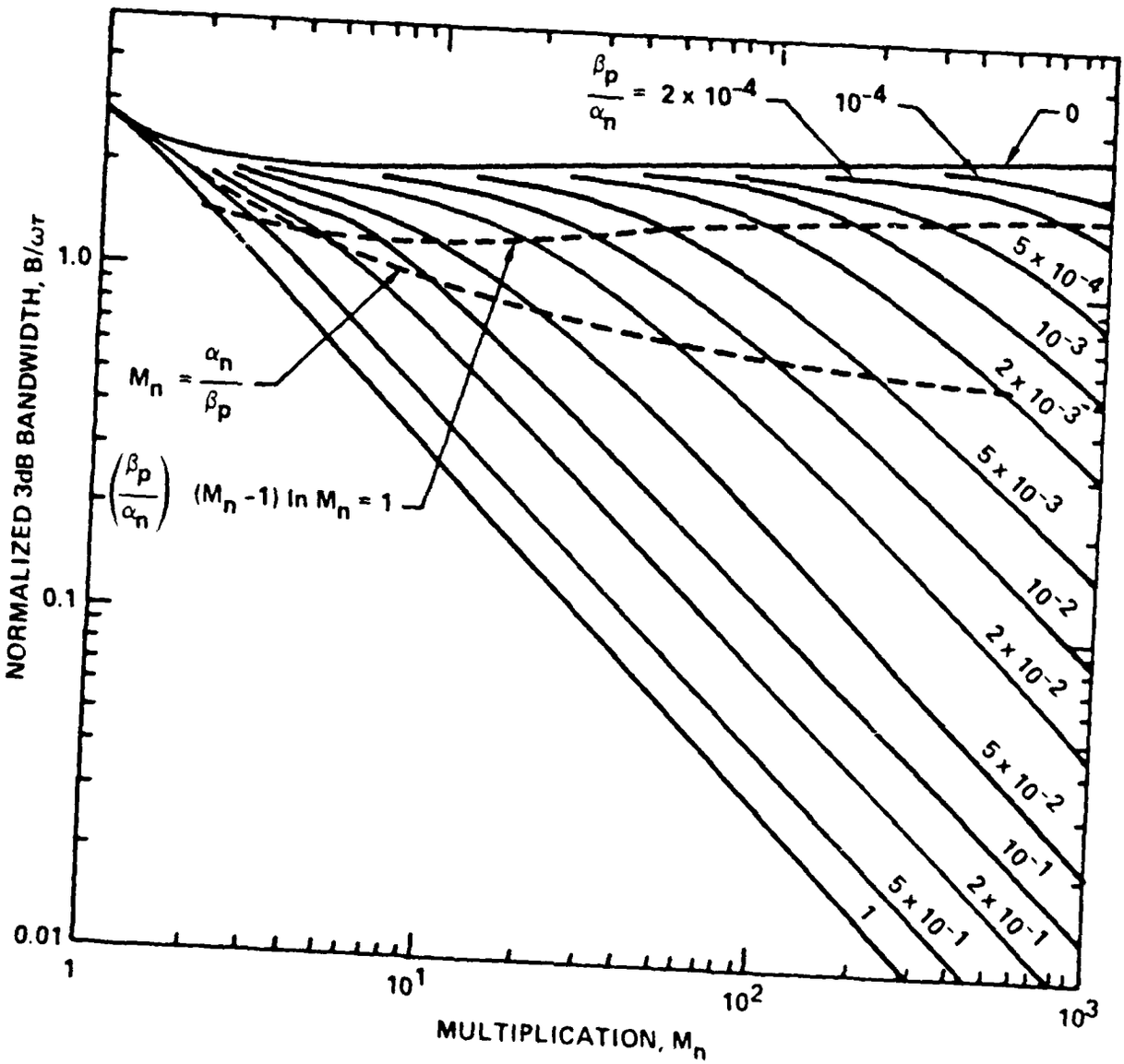

Fig. 2 Calculated 3 dB bandwidth of $F(\omega)$, normalized to $\omega\tau$, as a function of the dc multiplication of electrons injected at $x = 0$ for various values of β/α in a uniform electric field.

upon frequency response, although it does effect the noise performance.

Shown in Figure 3 are data taken from Logan and Sze[7] showing that GaAs has similar electron and hole ionization rates. The same trend is apparent in Figures 4 and 5 which show ionization data for InP[8] and InGaAsP[9], respectively. Note also that the $\beta/$ ratio exhibits its largest difference from unity at the lower electric fields where the ionization rate is also low.

1.3.2 Techniques of Enhancing α/β or α/β Ratios

One of the first proposals for a modification of α/β ratio by special device structure was a multistage structure of pn junctions arranged so that one carrier type (holes, for example) is preferentially trapped, while the other carrier type impact ionizes in the usual way.[10] Further consideration indicates that this device would not be suitable for a high speed detector. The problem is thermionic emission of the trapped carriers which would create a substantial tail on each pulse. Development of a different device structure first proposed by Chin, et al,[1] results in an enhancement of the ionization coefficient ratio and may also provide high speed is the focus of this program.

A diagram of the device structure proposed by Chin, et al,[1] under reverse bias conditions and its energy band structure are shown in Figure 6. The underlying physical ideas which originally led to expected enhancement of the ratio $/\beta$ in this structure are be explained as follows:

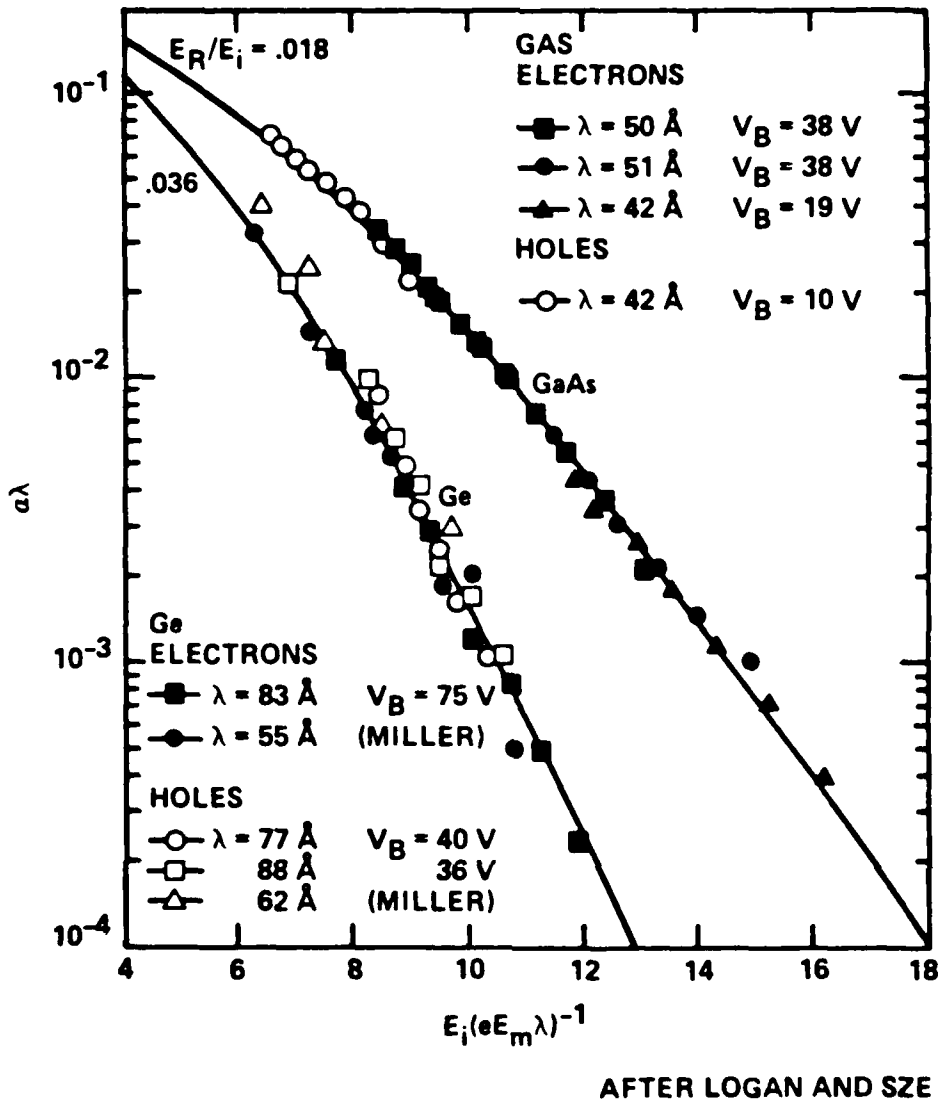

Fig. 3 Ionization rates of GaAs and Ge as a function of inverse electric field.

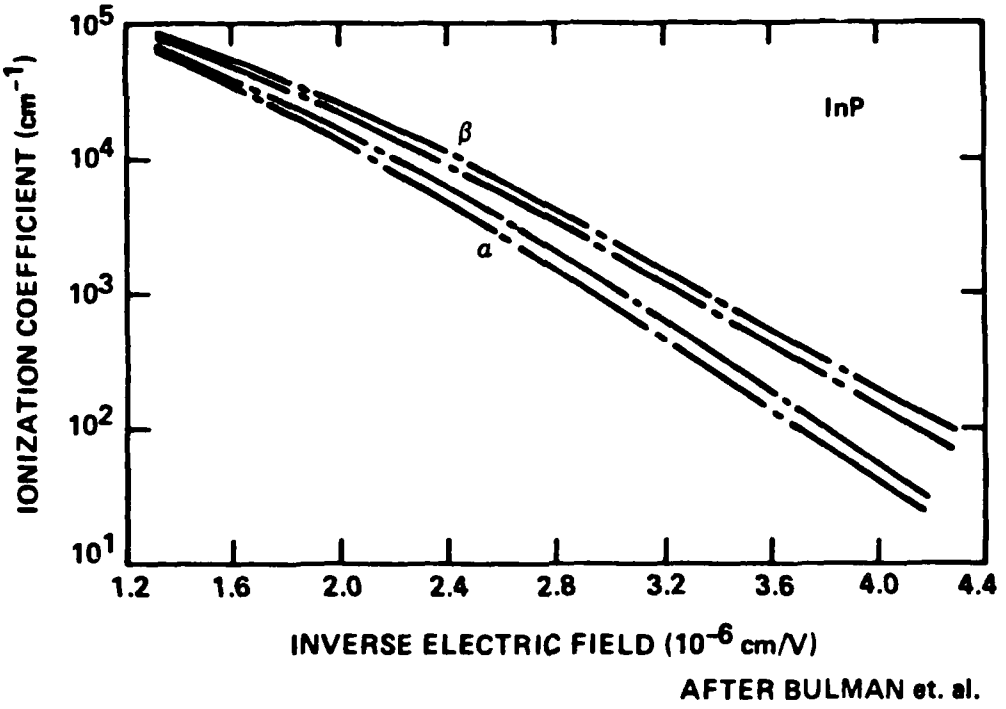

Fig. 4 Ionization rate of electrons and holes of InP as a function of inverse electric field.

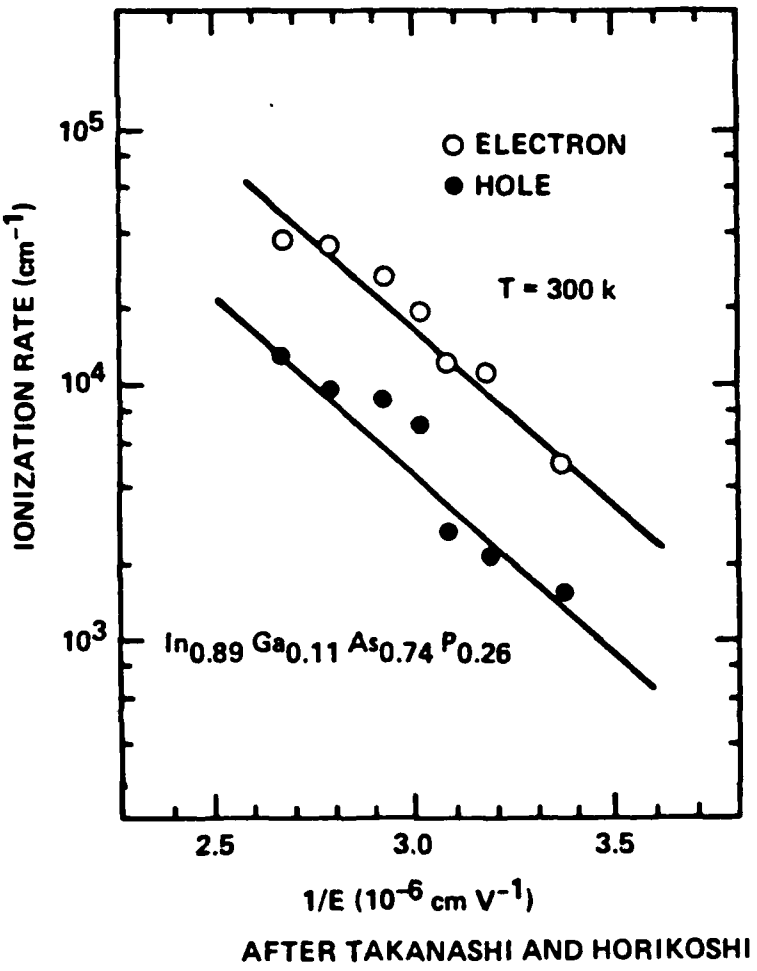

Fig. 5 Ionization rate for electrons and holes of InGaAsP as a function of inverse electric field.

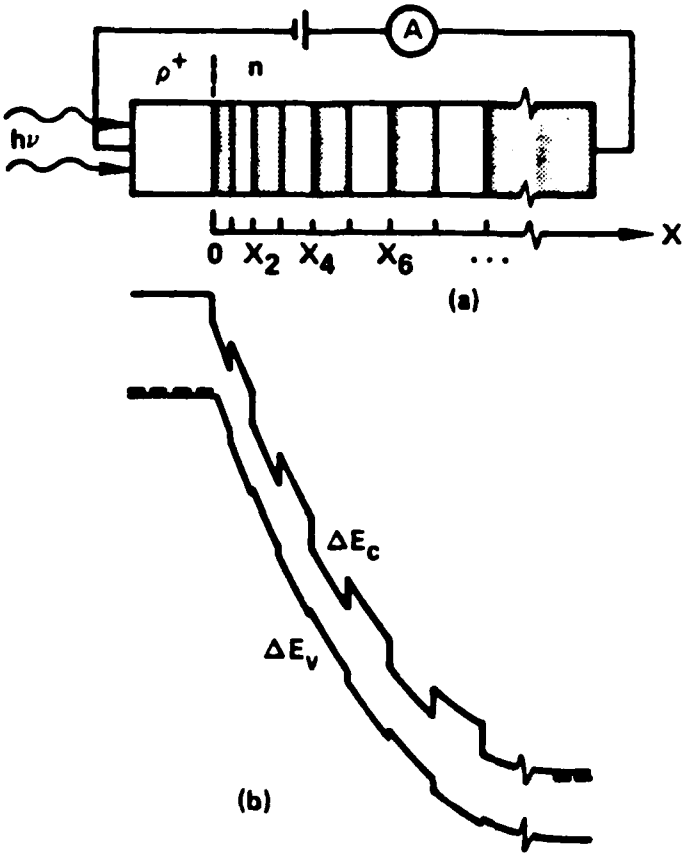

Fig. 6 Device and structure of a quantum well photodetector.

1. The impact ionization rate depends exponentially on the ionization threshold energy and on the energy from which the electron (hole) starts to be accelerated. Therefore, the step-like band structure shown in Figure 6, where the discontinuity in the conduction band is greater than that in the valence band, will enhance the ionization rate for electrons. A rigorous justification for this procedure can only be given for special cases, because in general the effect of the conduction band edge step on the ionization rate will depend on the energy which the electron already has when it approaches the junction.

2. As shown by Holonyak and co-workers,[11,12] the scattering rate in quantum wells is different from that in the bulk, and, at least at low energies, holes are scattered and collected more effectively in the quantum wells. An accurate analysis of this effect is difficult, because it must include the reflection and transmission through the (nonideal) heterojunction.

The above comments suggest that the α/β ratio can be substantially enhanced in quantum well structures, especially because of the second enhancement effect, the reduction of the phonon mean free path. Capasso, et al,[2] have used MBE growth techniques to fabricate a device with a structure like that in Figure 6 in the AlGaAs/GaAs alloy system. Their measurements show an enhancement of α/β with a value of $\alpha/\beta = 10$ at an electric field in the 2.1 to 2.7 x 10^5 V/cm range. Their results are shown in Figures 7 and 8.

Whether the electron or hole ionization rate is increased artificially will determine which type of carrier should be injected into the high field region. In the case of InP-InGaAsP, reports indicate that approximately 69% of the

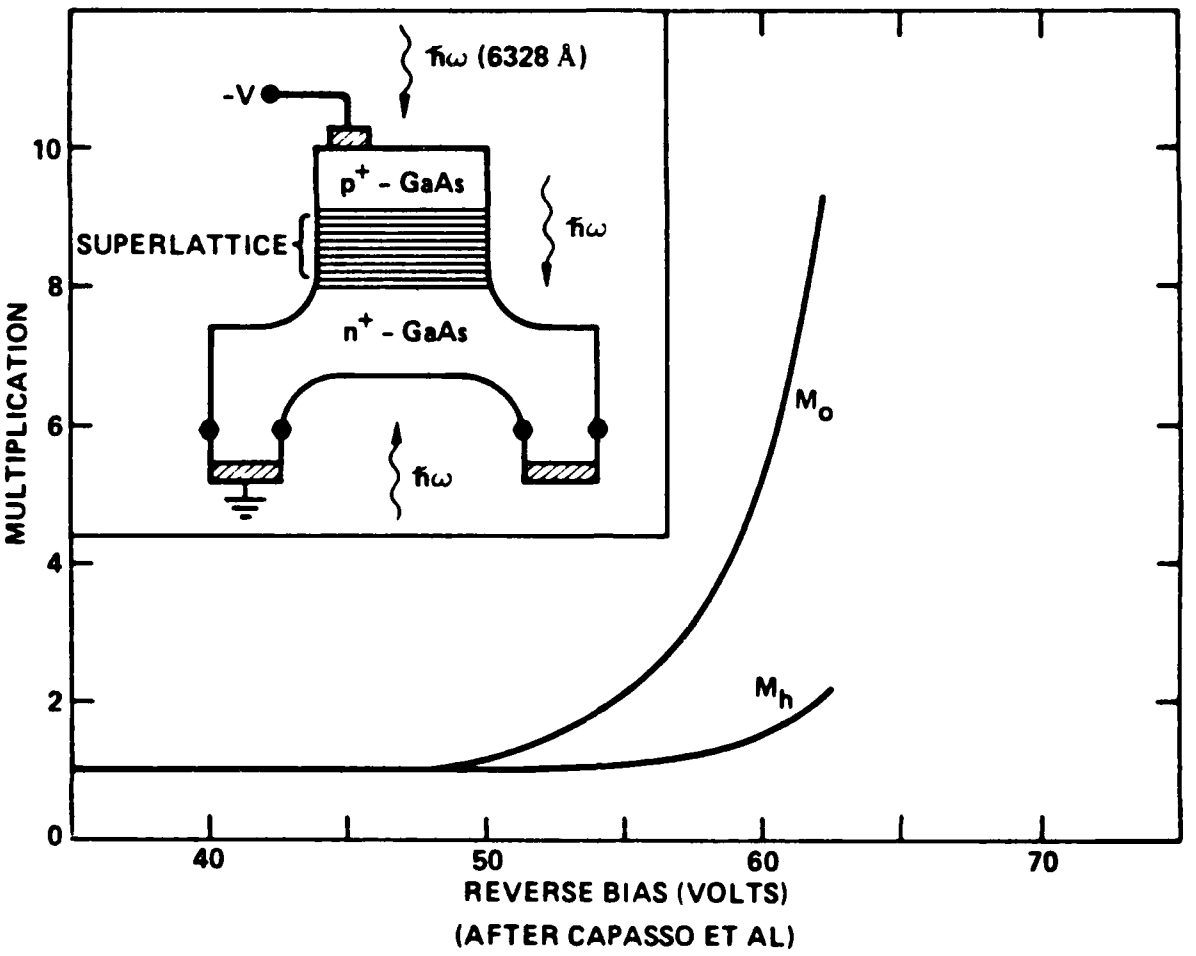

Fig. 7 Electron (M_e) and hole (M_n) initiated avalanche gain vs voltage. Shown in the inset is the device configuration.

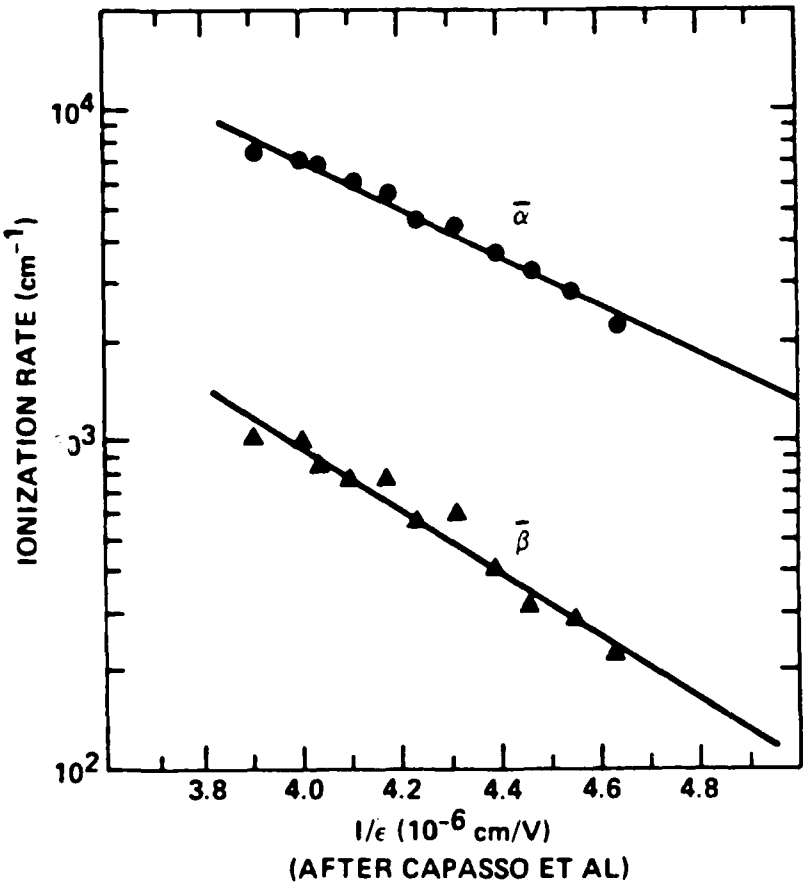

Fig. 8 Measured effective ionization coefficients for electrons ($\bar{\alpha}$) and holes ($\bar{\beta}$).

total discontinuity occurs in the valence band. In addition, measurements by Cook, et al,[13] show that β/α is approximately equal to four at low field values. Therefore, in this alloy system, the structure should be designed to provide hole injection as well as enhance the hole ionization rate above that of the electron rate to obtain the optimal avalanche photodetector.

2.0 PHASE 1 TECHNICAL PROGRESS

2.1 GaAs/AlGaAs Materials, Growth and Structure

2.1.1 Baseline PIN APD's

The initial device structures fabricated for this program were GaAs and AlGaAs avalanche photodiodes grown by metalorganic chemical vapor deposition (MOCVD). The first reported observations of significant avalanche gain in MOCVD grown devices were obtained from these structures. Gains of 7 to 8 were measured before substantial dark current was encountered. By employing continuous rather than interrupted growth during transitions from GaAs to AlGaAs layers, a decrease in dark current of over five orders of magnitude was obtained. Breakdown voltages were also found to increase dramatically in continuously grown devices compared to those grown discontinuously. The performance data from these devices provides the basis for comparison to similar data obtained later from devices containing GaAs/AsGaAs superlattice avalanche regions.

For the baseline structures, a simple p-i-n structure was chosen to obtain pure carrier injection. This structure is shown in Figure 9. Light absorption occurs completely within the top p-region allowing only electron injection to occur into the high field region.

In order to study the effects of growth conditions on gain, breakdown, and leakage current, a series of growth parameters were systematically explored. The aim was to reduce both deep and shallow impurity levels and also eliminate

STRUCTURE "A"
$Ga_{1-x}Al_xAs$ DETECTOR STRUCTURE

750Å	GaAs	$p \sim 3 \times 10^{17}$
1.5 μm	$Al_xGa_{1-x}As$	$p \sim 3 \times 10^{17}$
0.5 μm	$Al_xGa_{1-x}As$	p^+ 5 – 10 x 10^{17}
3.0 μm	$Al_xGa_{1-x}As$	UNDOPED
0.5 μm	$Al_xGa_{1-x}As$	$n^+ \sim 5 - 10 \times 10^{17}$
0.5 μm	GaAs	$n^+ \sim 1 \times 10^{18}$

GaAs SUBSTRATE

Fig. 9 Avalanche photodiode structure used for baseline devices. For the superlattice avalanche detectors, the GaAlAs undoped region is replaced by fifty alternating layers of GaAs and GaAlAs.

interface states. Deep impurity levels and interface states primarily affect the dark current by contributing to tunnelling of carriers through mid-gap states or levels. Shallow impurity levels affect the doping level and therefore the breakdown voltage, which in turn affects the gain.

Reduction of impurities is accomplished through both the use of high purity starting materials and establishment of growth conditions which minimize impurity incorporation. Relatively pure metalorganic trimethylgallium and trimethylaluminum from Alfa-Ventron was used. A mixture of 10% arsine in hydrogen was the arsenic source. Undoped GaAs mobilities of μ_{77} = 45,000 $cm^2/Vsec$ were obtained with these sources, demonstrating that the starting materials were of acceptable quality. No photoluminescence peaks were observed between 0.88 μm and 2.0 μm (the long wavelength detector limit) indicating the absence of large densities of deep impurity levels.

The other factors which affect impurity incorporation and interface state density are reactor construction and condition, gas phase stoichiometry (i.e., column three to five atom ration), growth temperature, growth rate, and whether the crystal growth is interrupted at any time during the epitaxial deposition process. This last factor was found to be especially important as is discussed below.

During the initial stages of the program, the reactor was helium leak tested and found to be leak free. A standard reactor purge or preconditioning procedure prior to crystal growth was used to ensure reproducibility. Some modifications were made to the reactor to eliminate memory effects caused by

the dopant gases. As a result of these precautions, uncontrolled impurity incorporation caused by the reactor geometry is felt to be minimal.

The main growth parameters were then examined for their effects upon device performance. These included growth rate, growth temperature, gas phase stoichiometry, and continuous vs. discontinuous crystal growth. The growth rate was varied from 375 Angstroms/min to 3,000 Angstroms/min, the growth temperature from 600C to 750C, and the gas phase stoichiometric III/V ratio from 10 to 20. Table 2.1 lists the samples grown, the conditions under which they were grown, and resulting device characteristics.

A comparison of the GaAs samples clearly indicates that a continuous growth procedure produces the best structures. For example, samples 3 and 11 were nearly identical in structure and grown under identical conditions except sample 11 has no interruptions in the growth process. Without interruption, the gain and breakdown voltage increase by a factor of two, and the dark current drops by five orders of magnitude. For some samples, gain was observed at leakage currents below 10 pA. This is illustrated in Figure 10 where dark current and light I-V characteristics of a GaAs APD are plotted.

For GaAlAs devices, a similar magnitude of dark current reduction was obtained by using the continuous growth procedure. Figures 11 and 12 show the dark and light I-V for GaAlAs avalanche photodiodes with AlAs mole fractions of 30% and 45%, respectively. Unfortunately, for the GaAlAs devices, even though the dark current showed a substantial reduction, the avalanche gain and breakdown voltage changes were not improved. For example, the continuously grown 45%

TABLE 2.1

SUPERLATTICE APD PROGRAM

Sample #	Growth Rate (R/min)	Growth Temp. °C	V/III Ratio	% Al	Interruption	V_{BR}	Gain	Structure	Leakage
B20210C	1500-3000	750	10-20	Superlat.	yes	30V	3-4	n^+-n-p^+	
B20617B	1500-2500	750	11-20	0.4	yes	50V	3-5	n^+-n-p	200 μA
B20617A	1500 Å	750	20	0.0	yes	45-50V	2-3	n^+-n-p	200 μA
B20618A	1500-3000	750	10-20	Superlat.	yes	30V	3-4	n^+-n-p	
B21029A	1500 Å	750	10-20	0.0	yes	40-60V	2-3	n^+n p	
B30301C	375 Å	775	20	0.0	yes	35-40V	2-4	p^+-n	
B30301B	375 Å	700	20	0.0	yes	35-40V	2-3	p^+-n(Zn sub)	
B30301A	375 Å	600	20	0.0	yes			p^+-n(Zn sub)	
B30711B	1500 Å	750	20	0.0	yes			p^+-n	
B30912B	750 Å	750	20	0.0	no	90V	7-9	A	
B30913B	750 Å	750	20	0.0	no	90V	6-7	A	
B30914A	375 Å	750	40	0.0	no	90V	7-8	A	0.1-10 nA
B30914B	750 Å	700	20	0.0	no	100V	7-8	A	0.0-10 nA
B31116A	750-1070	750	14-20	0.30	no	30V	4	A	0.5-5 nA
B31116B	750-1360	750	11-20	0.45	no	20V	4	A	0.1-2 nA
B31116C	750-1875	750	8-20	0.60	no	160V	*	A	*

* Not measurable due to field punchthrough into the substrate

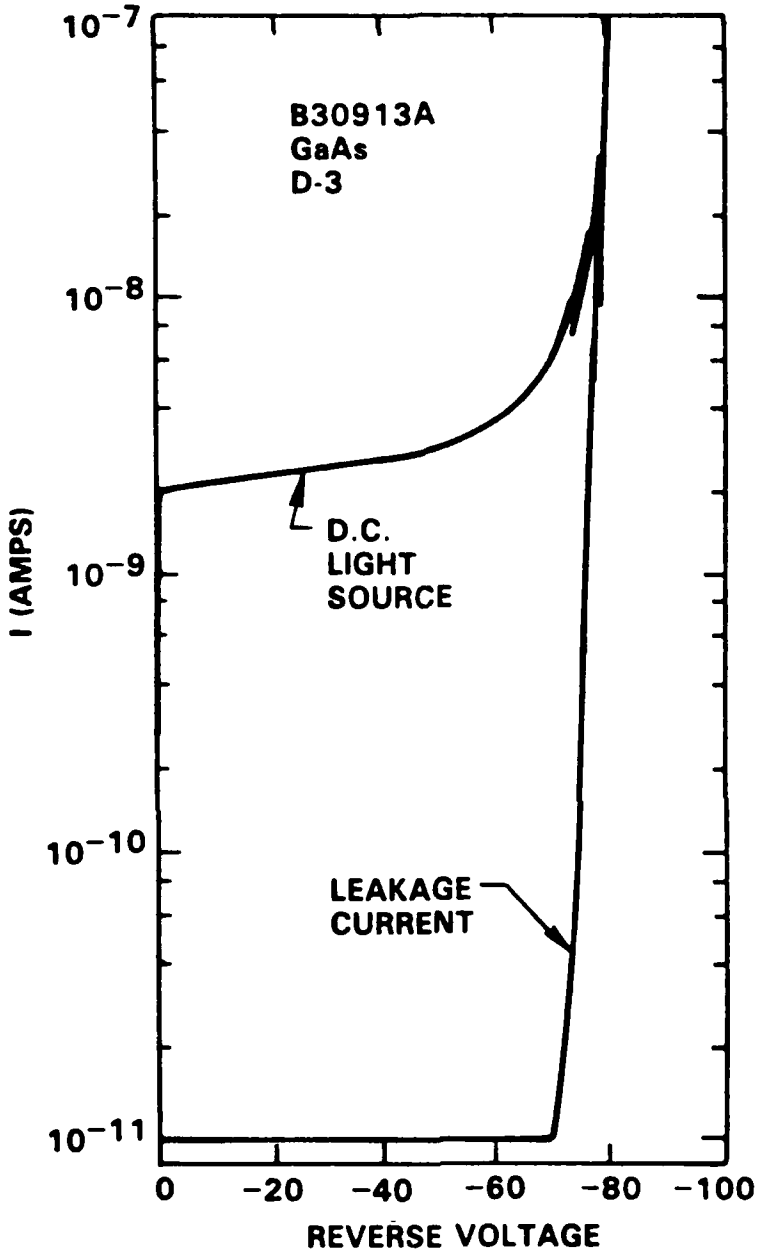

Fig. 10 Dark and light I-V characteristics of a MOCVD GaAs avalanche photodiode.

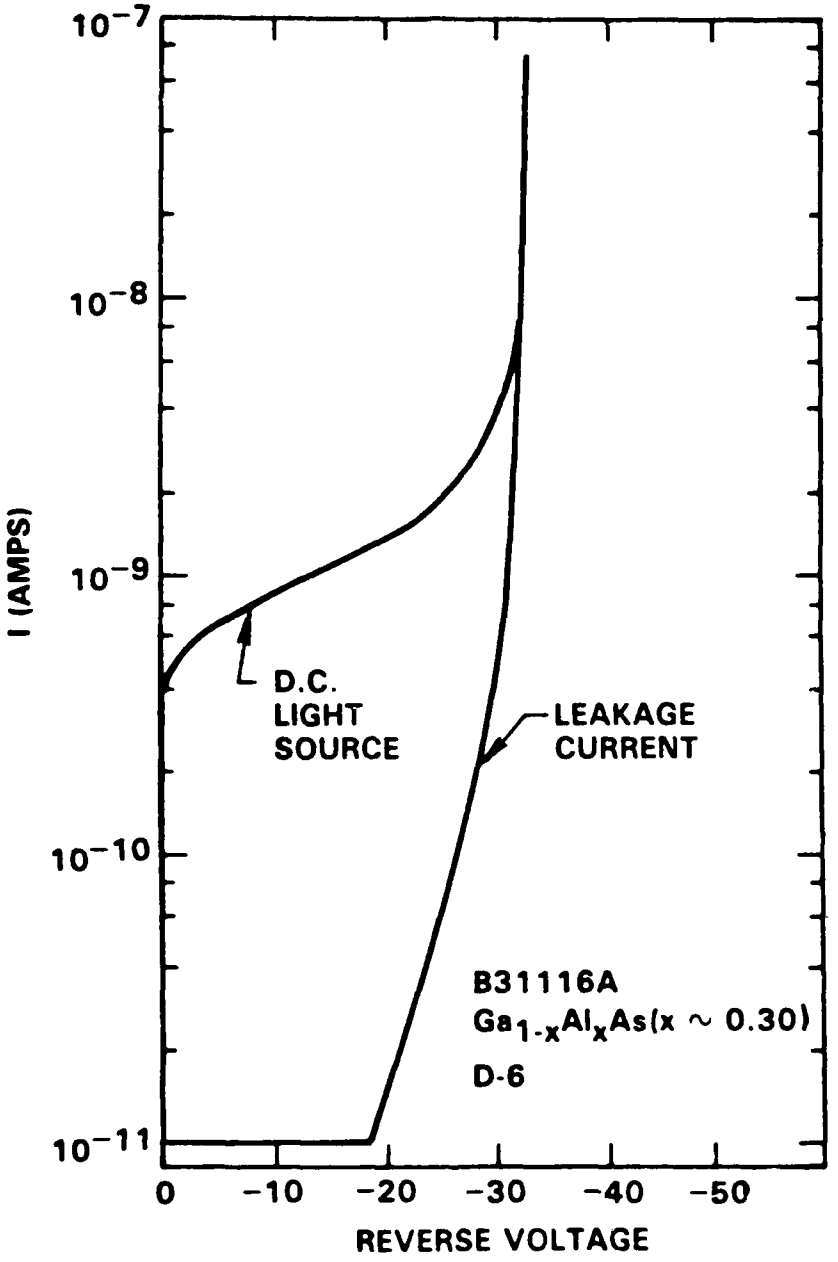

Fig. 11 Dark and light I-V characteristics of a MOCVD GaAlAs avalanche photodiode with a 0.30 AlAs mole fraction.

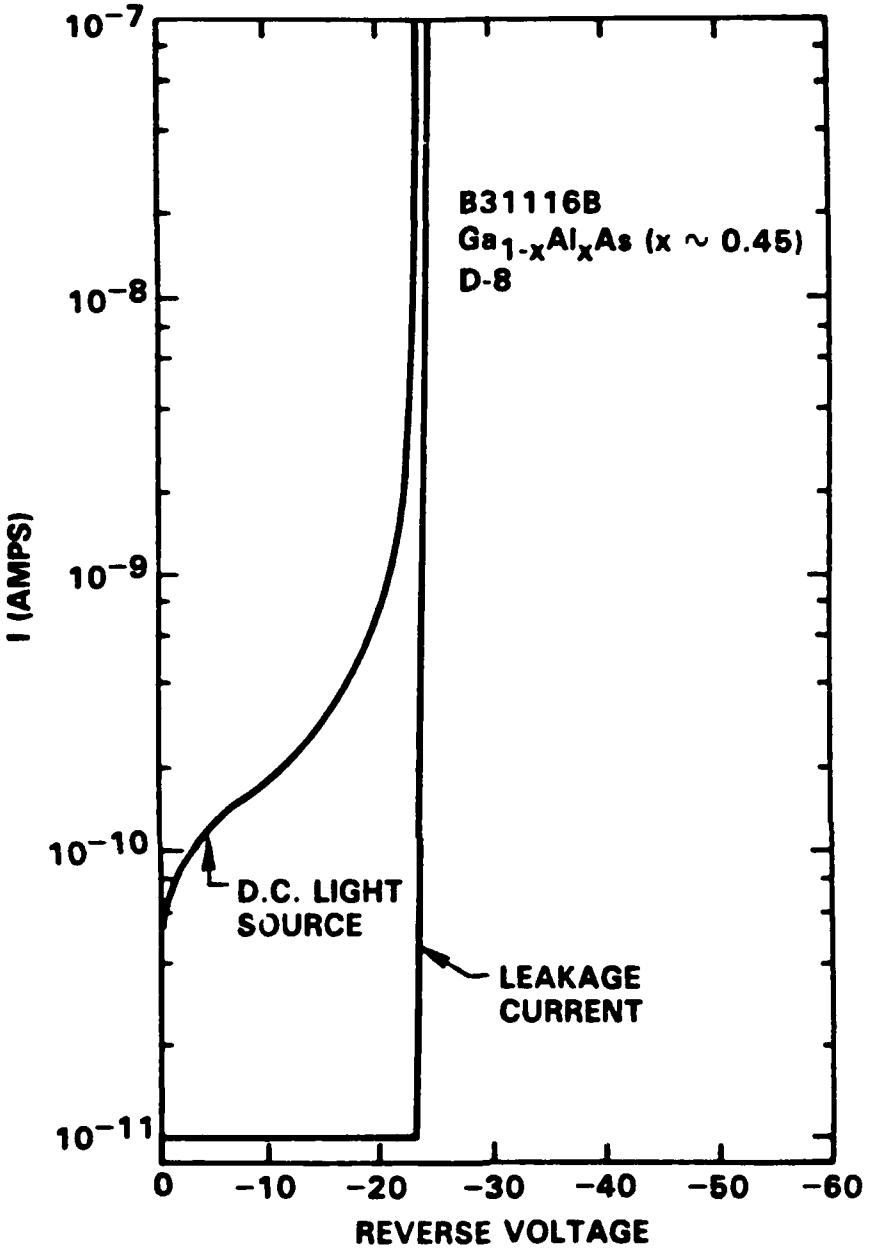

Fig. 12 Dark and light I-V characteristics of a MOCVD GaAlAs avalanche photodiode with 0.45 AlAs mole fraction.

AlAs mole fraction sample showed gain values which are no better than a 40% AlAs mole fraction sample grown by discontinuous deposition. In addition, the breakdown voltages in the 20 to 30 volt range were lower than expected. It is felt that the low breakdown voltages may be related more to the fundamental conduction band structure than to the issue of continuous vs. discontinuous growth.

For the 60% AlAs mole fraction sample, the dark current remained below 10 pA ($J_D < 10^{-7}$ A/cm^2) until breakdown. Due to equipment limitations, the dark current could not be measured below this value, and therefore it represents an upper found for J_D. Representative dark and light I-V plots are shown in Figure 13. The measured breakdown voltages of device of this material composition had values in excess of 160 volts. As a result, the gain could not be accurately measured due to the electric field punching through to the substrate and affecting the device absorption properties.

To help identify the source of the low breakdown voltage in the $Ga_{1-x}Al_xAs$ devices with x = 0.3 to 0.45, single $Ga_{1-x}Al_xAs$ epilayers in the composition range were grown on semi-insulating GaAs substrates. Hall measurements on layers having x = 0.3 indicated p-type background doping in the 3 - 4E16 cm^{-3} range. Similar measurements for x = 0.4 material indicated much lower impurity levels. Because dopant species at this composition of GaAlAs are not fully ionized at room temperature, the result is not directly comparable to data from lower Al content material. This is significant for APD applications because the degree of impurity ionization can be significantly increased under a high applied field (such as that used to obtain avalanche multiplication) and lead to breakdown at an unacceptably low voltage.

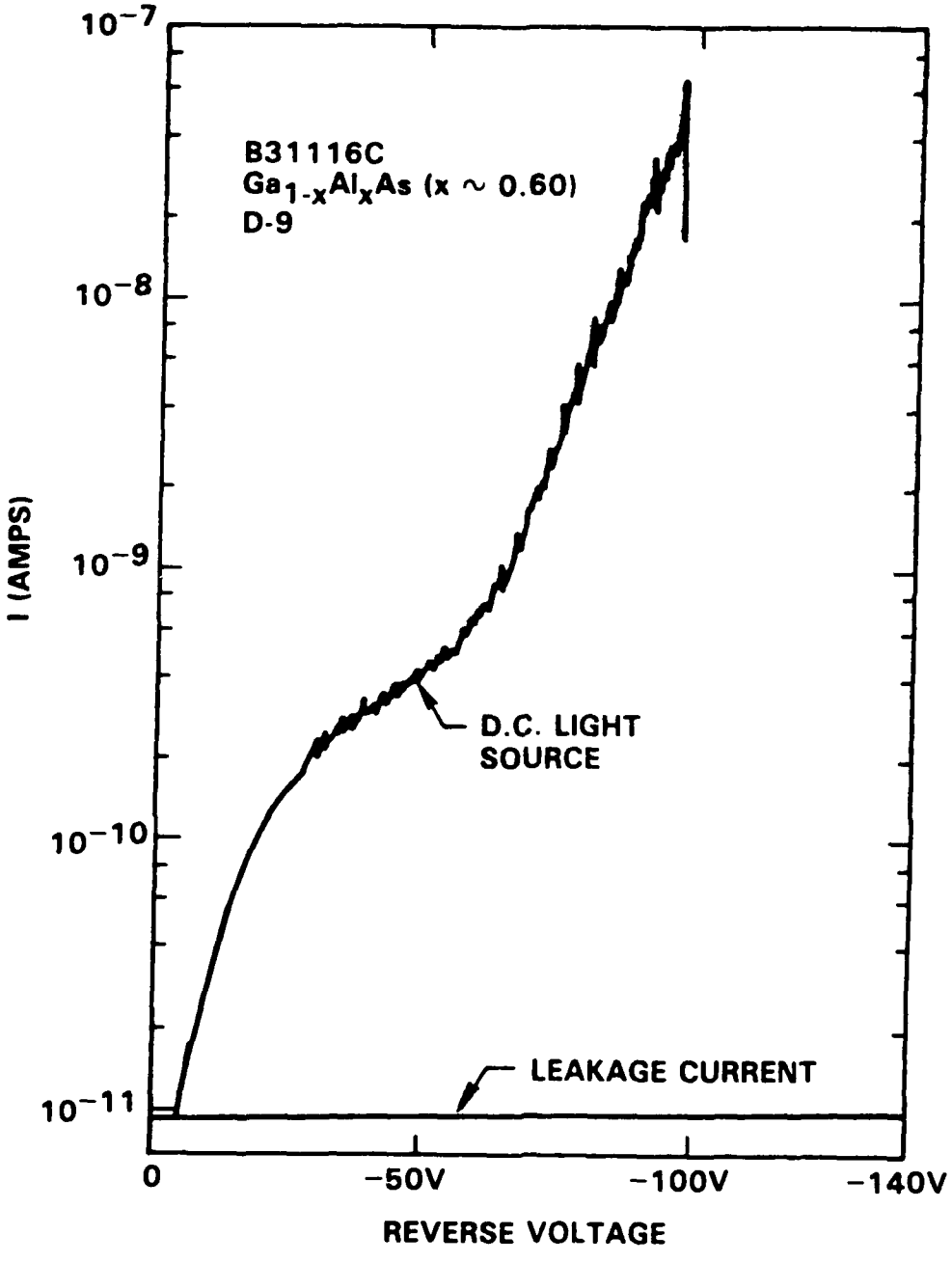

Fig. 13 Dark and light I-V characteristics of a MOCVD GaAlAs avalanche photodiode with 0.60 AlAs mole fraction. The breakdown voltage exceeds 160 volts.

It was thus necessary to further study the growth conditions for GaAlAs with the goal of impurity background reduction. The initial approach was to increase the V/III (AsH_3/TMG) ratio. This was intended to reduce the net impurity concentration by changing the background carbon to zinc ratio. Three GaAlAs homogeneous avalanche photodetector structures were fabricated with AlAs mole fractions of 0.30, 0.45, and 0.60 using V/III ratios in excess of 25. Upon testing, the measure gain of devices on any of the three wafers was less than two. The breakdown voltages, however, did increase slightly.

Upon further investigation, it was deterimend that the low gains were a result of a growth system calibration problem. The MOCVD reactor was not properly calibrated with respect to compositional control, and this resulted in inferior quality epitaxial layers. This conclusion was further corroborated by data taken upon GaAlAs/GaAs laser devices grown during the same period.

2.1.2 Superlattice APD Structures

Two superlattice avalanche photodiode structures were examined initially. The structures are the same as that of Figure 9, except the undoped GaAlAs region was replaced by 50 alternating layers of GaAs and AlGaAs with thicknesses of 450 Angstroms and 550 Angstroms, respectively. The outer cladding layers of GaAlAs have the same composition as the GaAlAs layers within the superlattice region. The two superlattice avalanche photodiode types had $Ga_{1-x}Al_xAs$ regions with AlAs mole fractions of 0.30 and 0.60.

Shown in Figures 14, 15, and 16 are SEM photomicrographs of the 0.60 AlAs mole fraction GaAlAs superlattice avalanche detector. The photographs show cleaved and etched cross sections of the mesa diode. In Figures 15 and 16, it is clearly evident that the period of the superlattice is 1,000 Angstroms and that there exists 50 interfaces in the high field region. Figure 17 shows the carrier concentration profile of a superlattice detector as determined from C-V measurements. The undulations are due to the different doping levels of the GaAs and GaAlAs layers.

One of the initial concerns was whether the leakage current would increase dramatically when a large number of heterostructure interfaces were present. Interface states are generally detrimental, since they act as generation centers for dark current. *With 50 interfaces, especially in a high field* region, such a problem could seriously degrade detector sensitivity. As shown in Figure 18, for a $Ga_{1-x}Al_xAs$ ($x \simeq 0.30$) superlattice avalanche photodiode, the dark current of the superlattice devices and their bulk homogeneous counterparts remains below the 10^{-11} amperes ($< 10^{-7}$ A/cm^2) detection limit of the measurement system until avalanche breakdown begins. This clearly demonstrates that interface states are acceptably low for the present GaAs and GaAlAs epitaxial layers grown by MOCVD. The light I-V characteristic of Figure 17 shows that gains of 3 to 4 are easily obtained with these devices. Shown in Figure 19 is the dark and light I-V of a $Ga_{1-x}Al_xAs$ ($x = 0.60$) superlattice avalanche photodiode. As in the previous case, the dark current is below the measuring capability of the ammeter (10^{-11} A) and only increases near avalanche breakdown. The undulations in the light I-V curve are similar to those observed by Capasso, et al,[2] on superlattice avalanche photodiodes

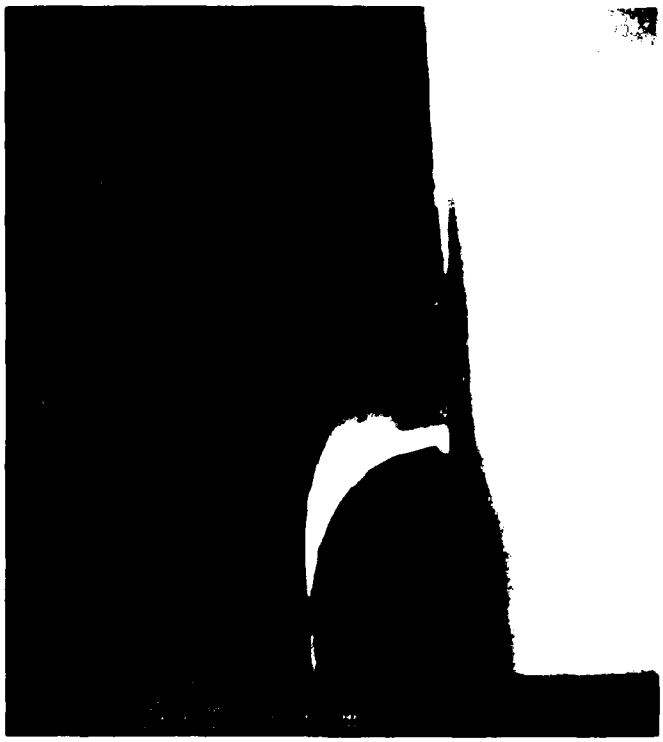

Fig. 14 SEM photograph of a cleaved cross-section of a GaAlAs-GaAs superlattice detector. The mesa corner is visible in the lower portion of the photograph.

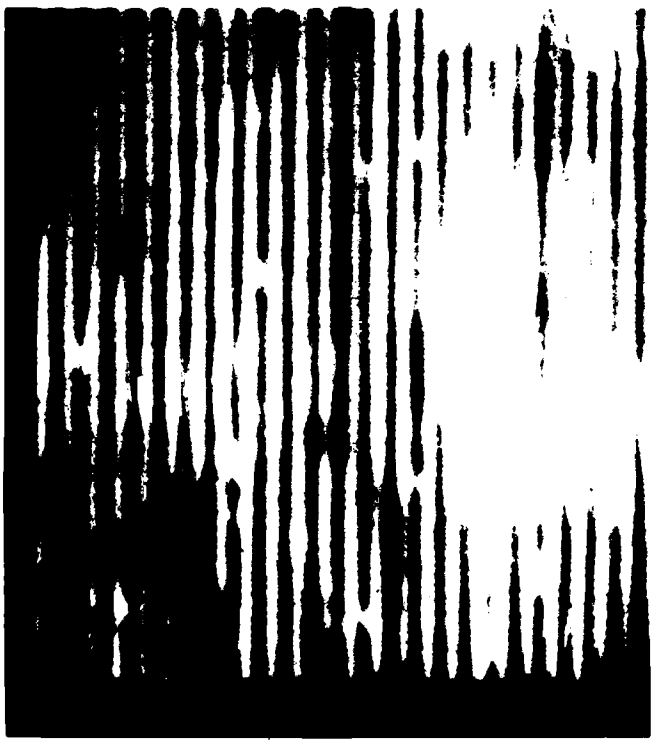

Fig. 15 SEM photomicrograph of a cleaved cross-section of the superlattice diode.

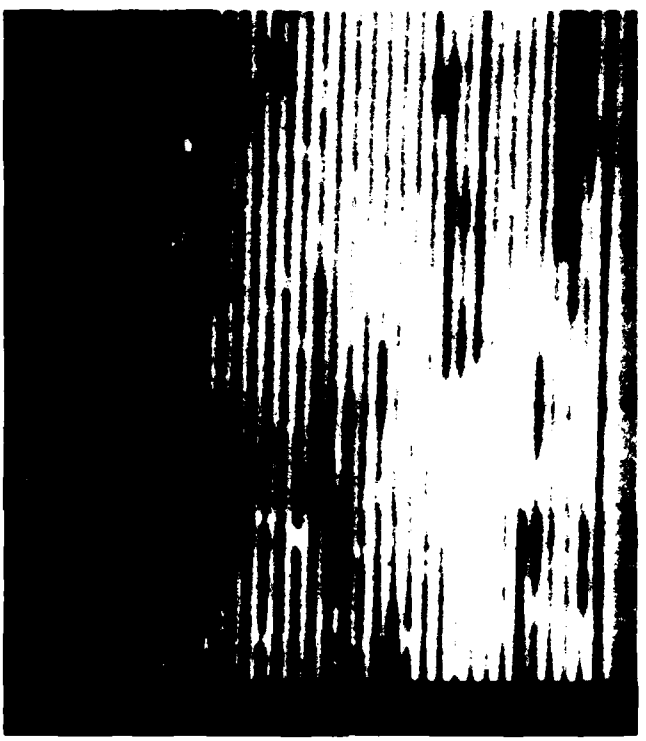

Fig. 16 SEM photograph of the superlattice region of the device of Fig. 17. Clearly visible is the 1000Å period. The GaAs and GaAlAs layers are 450Å and 550Å, respectively.

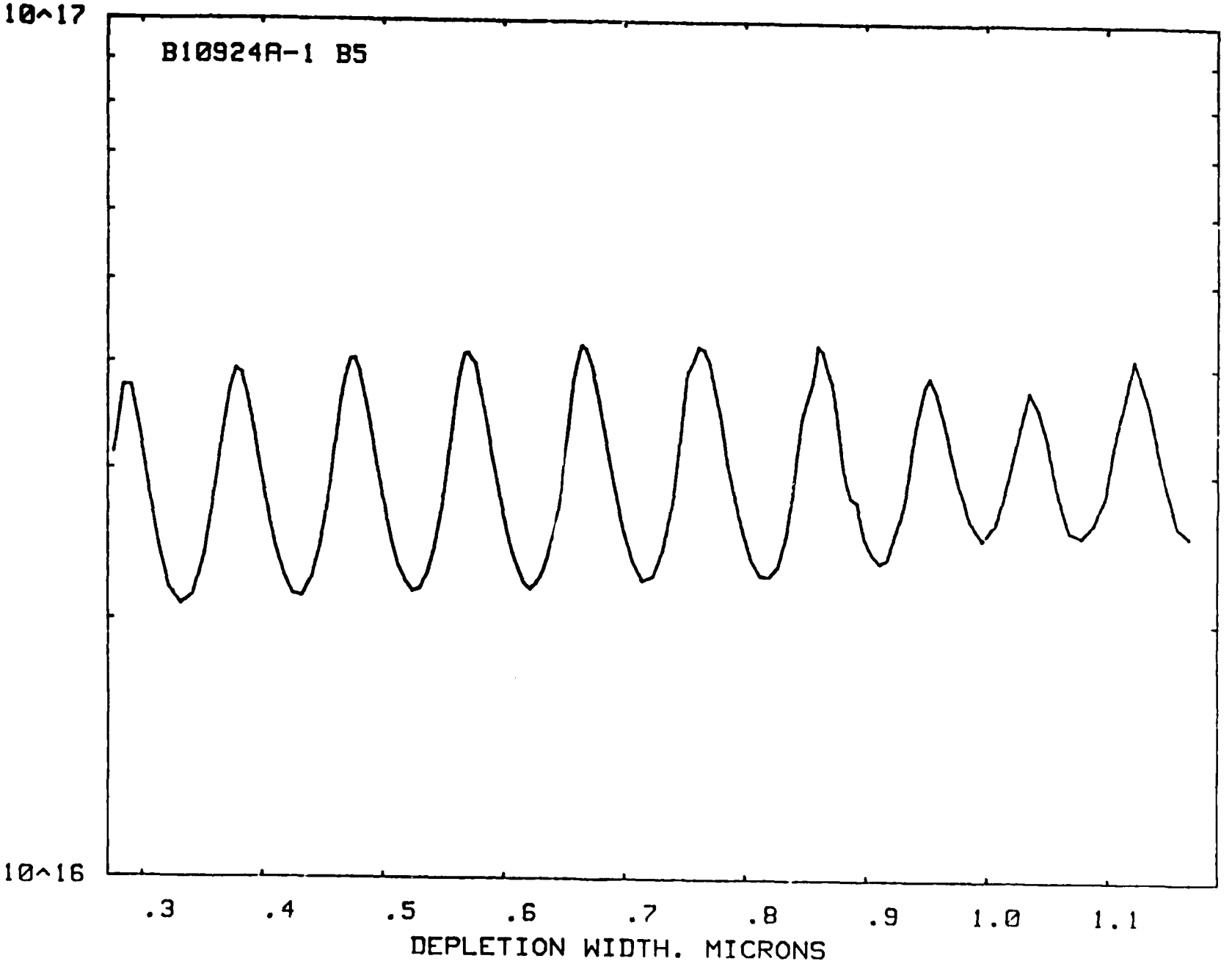

Fig. 17 Carrier concentration of a superlattice avalanche photodiode as determined from C-V profiling.

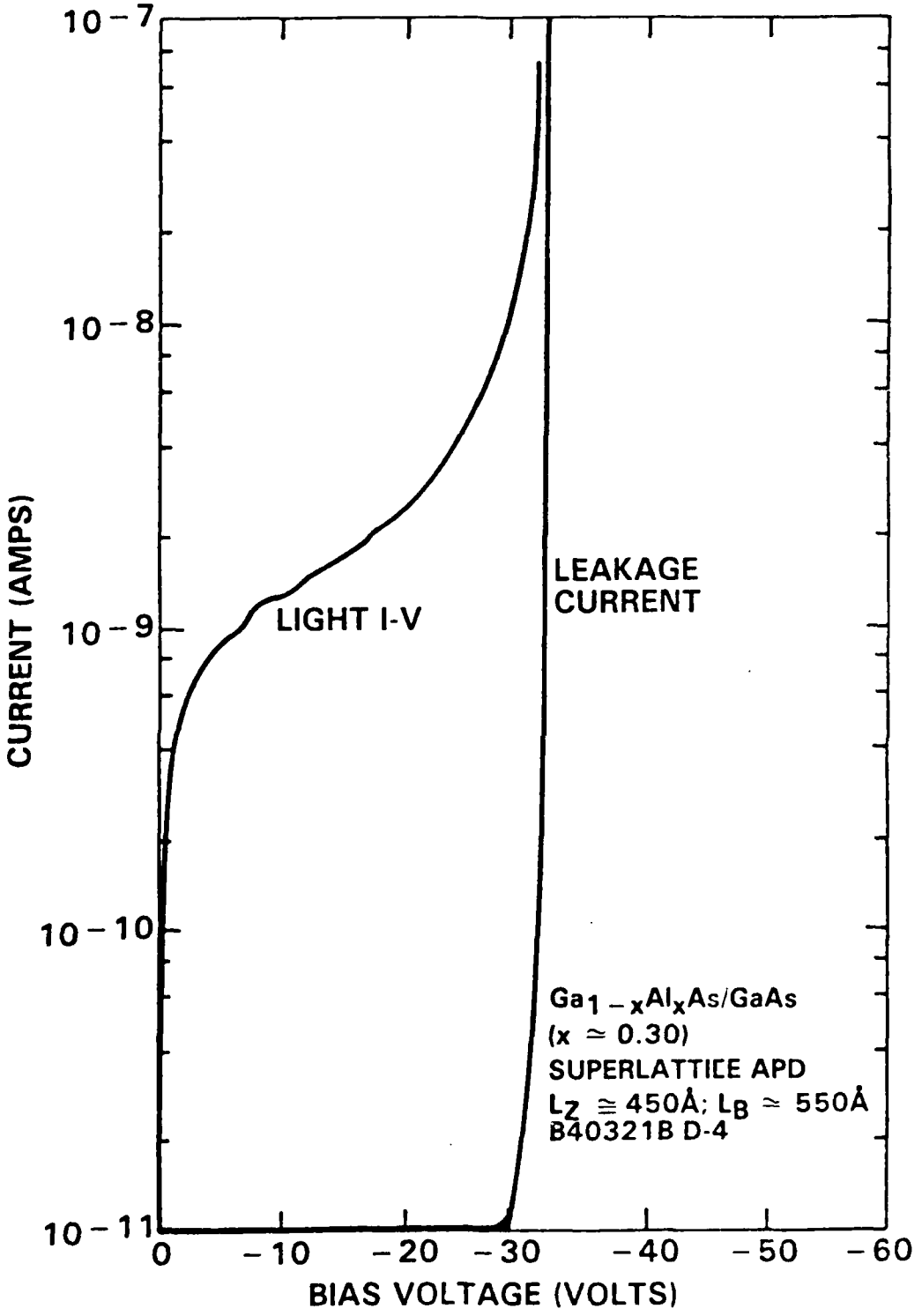

Fig. 18 Dark and light I-V of a $Ga_{1-x}Al_xAs$-GaAs ($x \simeq 0.30$) superlattice avalanche photodiode. The dark current remains well below 10^{-11} A until avalanche breakdown.

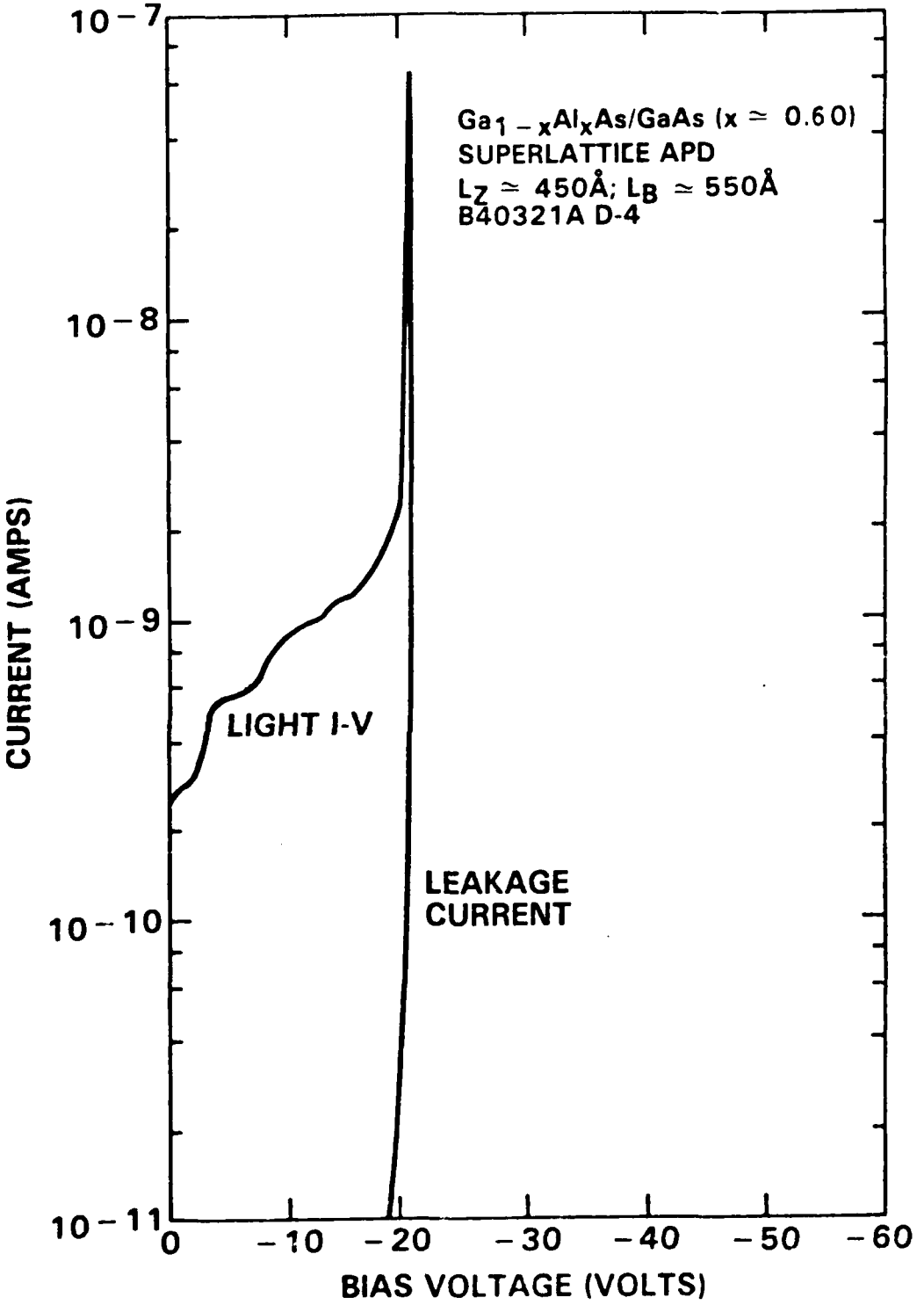

Fig. 19 Dark and light I-V of a $Ga_{1-x}Al_xAs$-Ga ($x = 0.60$) superlattice avalanche photodetector. The dark current remains well below 10^{-11} A until avalanche breakdown. This clearly demonstrates negligible interface states exist in these MOCVD grown photodiodes.

grown by MBE.

Although the breakdown voltage of the $Ga_{1-x}Al_xAs$ ($x \doteq 0.30$) superlattice may be explained by the background doping of the GaAlAs material, the breakdown voltage of the $Ga_{1-x}Al_xAs$ ($x \doteq 0.60$) material must be due to a different reason. As shown in the previous report, the breakdown voltage of $Ga_{1-x}Al_xAs$ ($x \doteq 0.60$) avalanche photodiodes were in excess of 150 volts. Similarly, the GaAs photodiodes exhibited breakdown voltages of approximately 90 volts. The conditions used to grow the previous $Ga_{1-x}Al_xAs$ ($x \doteq 0.60$) and GaAs avalanche photodetectors were employed in growing this superlattice avalanche photodiode. The breakdown voltage (where gain is measured) occurs on a number of devices and is, therefore, not an isolated phenomenon.

A second series of wafer having the general structure shown in Figure 9 was grown next to further explore the influence of several growth, composition and structural parameters on the optical and electrical characteristics of AlGaAs/GaAs super-lattice avalanche photodetector devices. The specific growth parameters varied were:

1. Aluminum content of both the photon absorption and S.L. avalanche regions.
2. MOCVD growth temperature.
3. Ga/As reactant ratio during MOCVD growth.
4. Total thickness of superlattice avalanche region.
5. Thickness of AlGaAs layers in the superlattice structure.

A total of nine structures were produced in this second series. Five of these structures were processed into mesa devices and characterized with respect to dark and illuminated current-voltage response and gain.

Because of the extremely low dark currents typical of these structures, a sensitive, automated measurement system having picoamp current measurement capability was assembled, programmed, and used for their characterization.

The best performance obtained from this series with regard to high breakdown voltage combined with low dark current and high gain, came from mesa devices on two of the wafers having differing Al compositions. The best and typical values of illuminated breakdown voltage, $V_{BDillum}$, dark current, I_{dark}, at 0.9 $V_{BDillum}$, and gain, Mph, at 0.9 $V_{BDillum}$ for these two wafers are summarized in Table 2.2. Two measures of gain are quoted. Mph is the photo multiplication factor defined as:

$$Mph(V) = \frac{I_{illum}(V) - I_{dark}(V)}{I_{illum}(V_{ref}) - I_{dark}(V_{ref})}$$

where

$I_{illum}(V)$ = Total (light and dark) current measured at bias voltage V.

$I_{dark}(V)$ = Dark current measured at bias voltage V.

$I_{illum}(V_{ref})$ = Total current measured at a low reference voltage well below the threshold of avalanche multiplication. (Typically $V_{ref} = -10$ V).

$I_{dark}(V_{ref})$ = Dark current measured at the reference voltage.

M is the multiplicaton factor defined simply as $M = I_{illum}(V)/I_{illum}(V_{ref})$.

Table 2.2

Summary of Performance Parameters for Best and Typical Superlattice Devices

Wafer No.	Mesa No.	Al Fraction of AlGaAs	$V_{BDillum}$ (Volt)	I_{dark} at 0.9 $V_{BDillum}$ (Amp)	Mph Photomultiplication Factor at 0.9 $V_{BDillum}$	Multiplication Factor M 0.9 $V_{BDillum}$	V_{ref} Volt
B40515A (best)	03P00P	0.30	-98	2.1E-9	1E4*	220	-10
B40718A (best)	06N04N	0.45	-80	1.2E-9	9E5*	7E6	-10
B40515A (typical)	01P04N	0.30	-89	9E-10	100	110	-10
B40718A (typical)	P02N04	0.45	-45	2.5E-9	41	200	-10

*May be anomalously high due to localized breakdown.

The full dark and illuminated log I vs V curves for these devices are shown in Figures 20(a) through 23(a) as noted. The corresponding photomultiplication factor vs bias voltage plots appear in Figures 20(b) through 23(b). The very high gain calculated for the best mesa measured on wafer B40718A, Figure 21(b), is a consequence of the rapid increase in I_{illum} beyond about - 30 V bias. This rapid photocurrent increase may be due at least in part to localized soft breakdowns associated with microplasma formation. More detailed studies of excess noise behavior and spatial gain uniformity are needed to determine the true level of useful gain for devices of this type.

The photocurrent curve (Figure 20(a)) for the best mesa of wafer B40515A shows little, if any, indication of breakdown of any sort for biases out to -100 V. The high gains calculated for this device may well be legitimate values, but again additional measurements are needed.

A summary of the growth and structual details of all the wafers grown during this report period is given in Table 2.3. A summary of the characteristic $V_{BDillum}$, I_{dark}, at 0.9 $V_{BDillum}$, and Mph at 0.9 V_{BD} for those 5 wafers which were processed into mesa devices is given in Table 2.4.

Within the As/Ga ratio = 33 growth series, all but one of the structures was grown at a 750°C temperature. A single structure (B40516A) having X_{Al} = 0.3 was grown at 700°C. Several mesa devices from this latter structure exhibited multiple (usually 2, occasionally 3) partial breakdowns under illumination. An example of this behavior is given by the dark and illuminated log I-V curves appearing in Figure 24(a). The partial breakdowns are believed due to local

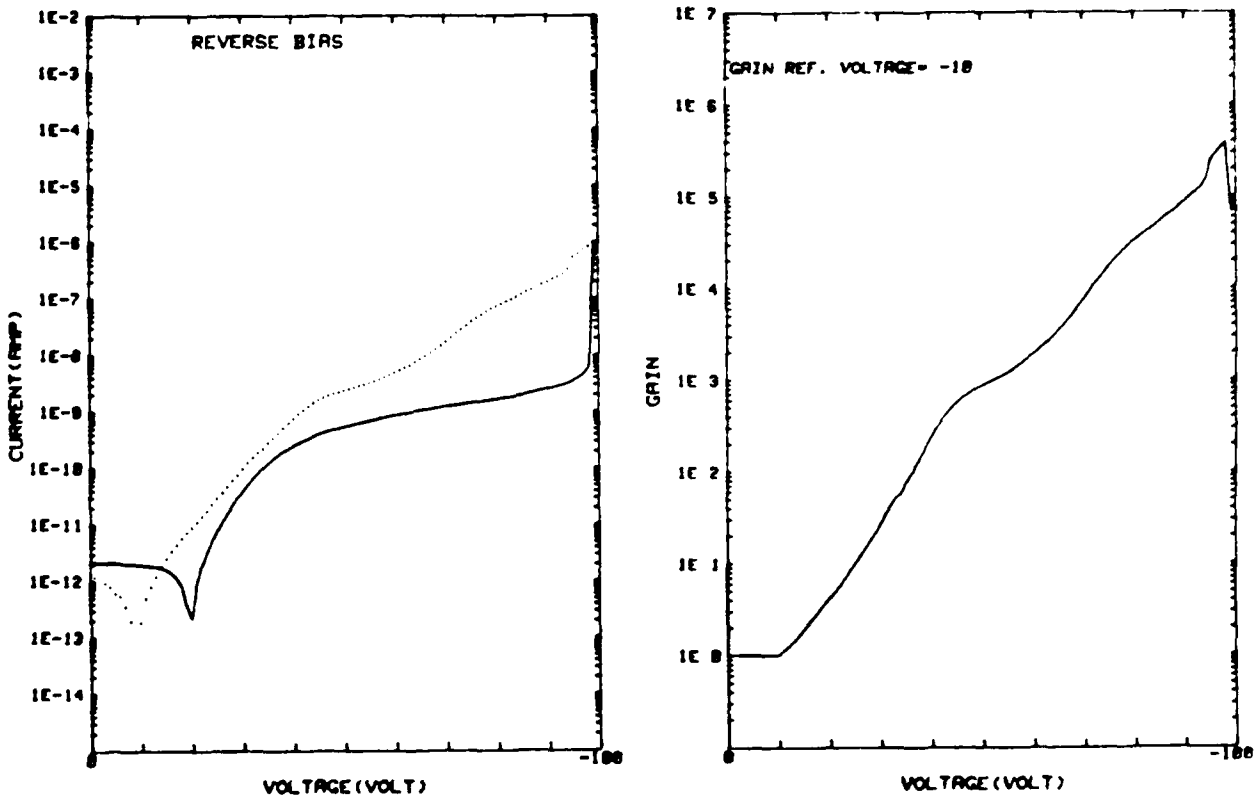

Fig. 20 (a)Light (dotted line) and dark (solid line) log I-V for best mesa device measured on wafer B40515A. (b) Calculated gain (photomultiplication factor) curve for the device of Fig. 2a.

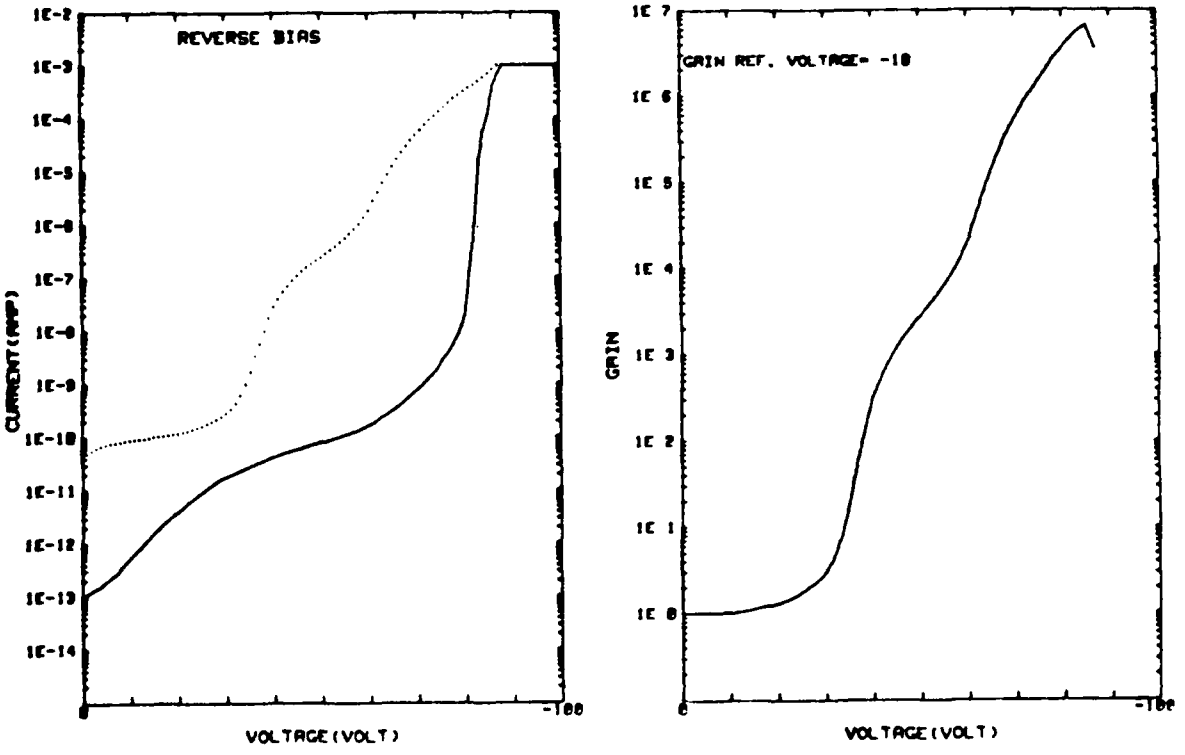

Fig. 21 (a) Light (dotted line) and dark (solid line) log I-V curves for best mesa device measured on wafer B40718A. (b) Calculated gain (photomultiplication factor) curve for the device Fig. 3a.

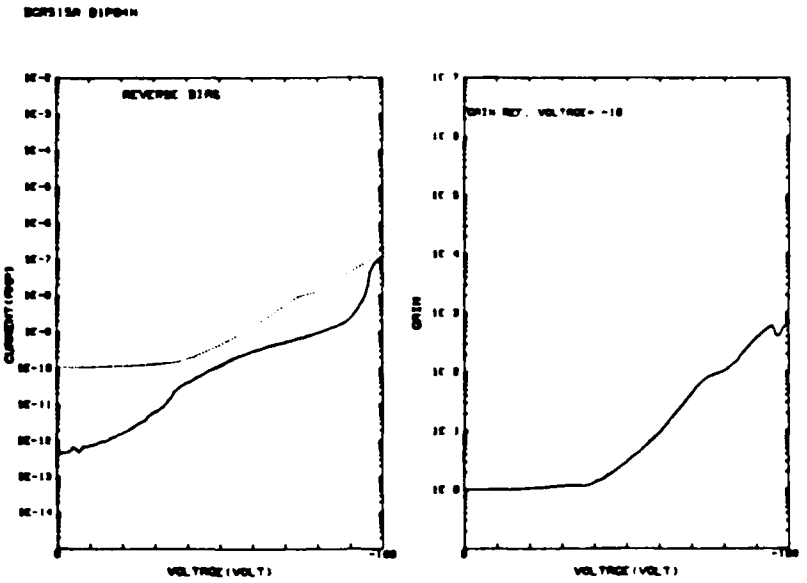

Fig. 22 (a) Light (dotted line) and dark (solid line) log I-V curves for typical mesa device measured on wafer B40515A. (b) Calculated gain (photomultiplication factor) curve for the device of Fig. 4a.

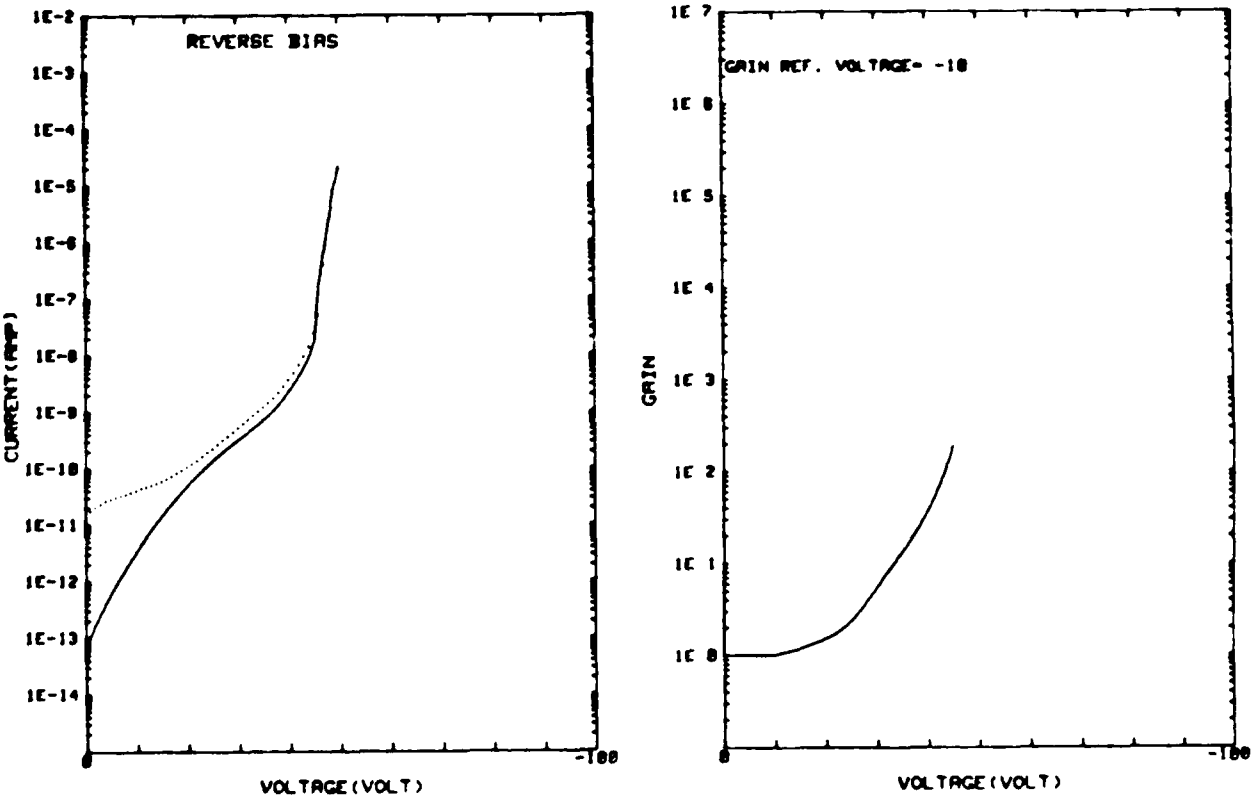

Fig. 23 (a)Light (dotted line) and dark (solid line) log I-V curves for typical mesa device measured on wafer B40718A. (b) Calculated gain (photomultiplication factor) curve for the device of Fig. 5a.

Table 2.3

Summary of Superlattice Growths and Their Growths/Structural Details

	Wafer No. Substrate: GaAs:Si 1E18	Growth Temp (°C)	Ga/As Ratio	Layer 1 Comp. X_{Al}:Dopant	Layer 1 Thickness (μm)	Layer 2 Comp. X_{Al}:Dopant	Layer 2 Thickness (μm)	S.L. or 1 Region X_{Al}	S.L. or 1 Region AlGaAs Thickness (Å)	S.L. or 1 Region GaAs Thickness (Å	S.L. or 1 Region Total Thickness (μm)
Al.6	B40222A	750	20	0.0:Se	0.4	--	--	0.6	425	450	2.3
Al.6	B40315B	750	20	0.0:Se	0.4	--	--	0.6	534	450	2.4
Al.6	B40321A	750	20	0.0:Se	0.2	0.6:Se	0.3	0.6	425	450	2.3
Al.3	B0321B	750	20	0.0:Se	0.2	0.3:Se	0.4	0.3	425	450	2.3
Al.3	B40515A	750	33	0.0:Se	0.2	0.3:Se	0.4	0.3	425	450	2.2
Al.3	B40516A	700	33	0.0:Se	0.2	0.3:Se	0.4	0.3	425	450	2.2
Al.45	B40718A	750	33	0.0:Se	0.2	0.45:Se	0.4	0.45	429	450	2.2
Al.6	B40718B	750	33	0.0:Se	0.2	0.6:Se	0.4	0.6	425	450	4.7
Al.3	B40801B	750	33	0.0:Se	0.2	0.3:Se	0.4	0.3	425	450	2.1

Layer 3 Comp. X_{Al}:Dopant	Layer 3 Total Thickness (μm)	Layer 4 Comp. X_{Al}:Dopant	Layer 4 Thickness (μm)	Layer 5 Comp. X_{Al}:Dopant	Layer 5 Thickness (μm)	Layer 6 Comp. X_{Al}:Dopant	Layer 6 Thickness (μm)
0.0:Zn^+	0.4	0.0:Zn	1.2	--	--	--	--
0.0:Zn^+	0.4	0.0:Zn	1.2	--	--	--	--
0.6:Zn^+	0.3	0.6:Zn	1.0	0.0:Zn	0.06	--	--
0.3:Zn^+	0.4	0.3:Zn	1.2	0.0:Zn	0.06	--	--
0.3:Zn^+	0.4	0.3:Zn	1.2	0.0:Zn	0.06	--	--
0.3:Zn^+	0.4	0.3:Zn	1.2	0.0Zn	0.06	--	--
0.45:Zn^+	0.4	0.45:Zn	1.2	0.0:Zn	0.06	--	--
0.6:Zn^+	0.4	0.6:Zn	1.2	0.0:Zn	0.06	--	--
0.3:Zn^+	0.4	0.6:Zn	1.2	0.0:Zn	0.06	0.45Zn+	0.09

Table 2.4

Summary of Performance Parameters Measured on
AlGaAs/GaAs S.L. Detector Structures

Wafer No.	Al Fraction	$V_{BDillum}$ (Volt)	I_{dark} at 0.9 $V_{BDillum}$ (Amp)	Photomultiplication Factor at 0.9 $V_{BDillum}$	As/Ga Ratio	Growth Temp. (°C)
B40315B	0.6	-10 to 11.5 (Av. = -10.9)	2E-11 to 1.3E-9 (Av. =7.9E-10)	1.6 to 3.0 (Av. = 2.1)	20	750
B40515A	0.3	-79 to -98 (Av. = -86.3)	6E-11 to 2.1E-9 (Av. =8.7E-10)	43 to 10,000 (Av. = 2,524)	33	750
B40516B	0.3	Multiple Partial Breakdowns* Under Illumination			33	700
B40718A	0.45	-32 to <-100 (Av. -65)	1.2E-11 to 2.5E-9 (Av. = 8E-10)	9 to 5E6 (Av. = 1E6)	33	750
B40718B	0.60	-34 to -37.5 (Av. = -35.9)	1.2E-12 to 9E-10 (Av. = 2.3E-10)	14 to 100 (Av. = 40.6)	33	750

*Mesas devices showed 2 (occasionally 3) sharp increases in total illumination current.
Typical bias levels for partial breakdowns were ~ -20; -48; -72 V.
Typical I dark values at 0.9 $V_{BDillum}$ were 2 to 3E-11, ~ 2.8E-10, 2.8E-10 to 3.2E-9 amp.
Typical gain values at 0.9 $V_{BDillum}$ were 1.5-2.3; ~ 40; 70-9E5.

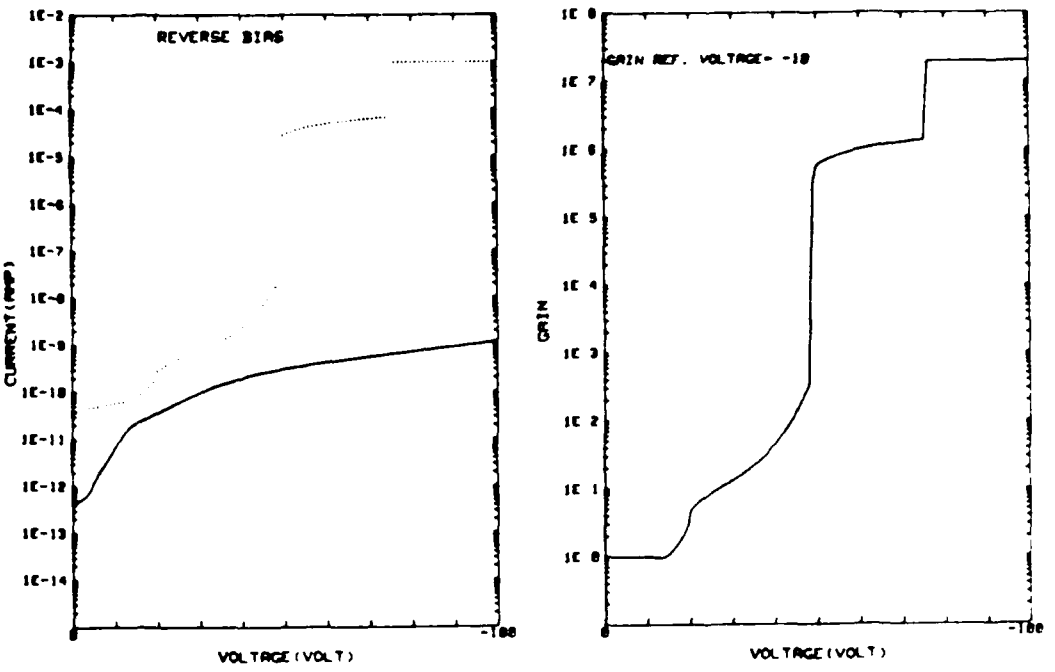

Fig. 24 (a) Light (dotted line) and dark (solid line) log I-V curves showing multiple breakdowns under illumination typical of many devices from the $Al_{0.3}Ga_{0.7}As/GaAs$ S.L. structure grown at 700°C (wafer B40516A). (b) Calculated gain (photomultiplication factor) curve for the device of Fig. 6a.

microplasma formation associated with structual inhomogeneities. It is speculated that the structural inhomogeneities result from the inferiority of $Al_{0.3}Ga_{0.7}As$ material (i.e., higher trap and defect densities grown by MOCVD at temperatures below 750°C.

The gain vs bias curve for this multiple breakdown mesa device appears in Figure 24(b). The exceptionally high, nearly constant gain region occurring between -50 and -75 V, is probably well outside the range of usefully low excess noise generation. Beyond -75 V, the true I_{illum} is outside the current limit of the measurement apparatus.

The $Al_{0.6}Ga_{0.4}As$ structure grown with the (low) As/Ga ratio of 20 consistently yielded devices having $V_{BD} \sim$ -11 V AND Mph ~ 2.0. A set of log I-V and photomultiplication gains vs bias voltage curves for a typical device from this wafer are shown in Figures 25(a) and 25(b), respectively. This low breakdown voltage is consistent with results obtained earlier in this program for homogeneous AlGaAs p-i-n detector structures grown at this lower As/Ga ratio. Based on these results, work with other samples from the low As/Ga ratio growth series was halted to allow full concentration of effort on the more promising samples from the As/Ga = 33 series. All but the most recently grown of the high As/Ga ratio wafers (B40801B) were processed and characterized during this report period.

In an effort to better understand the measured characteristics of the present series of devices, calculations were done to estimate the distribution of

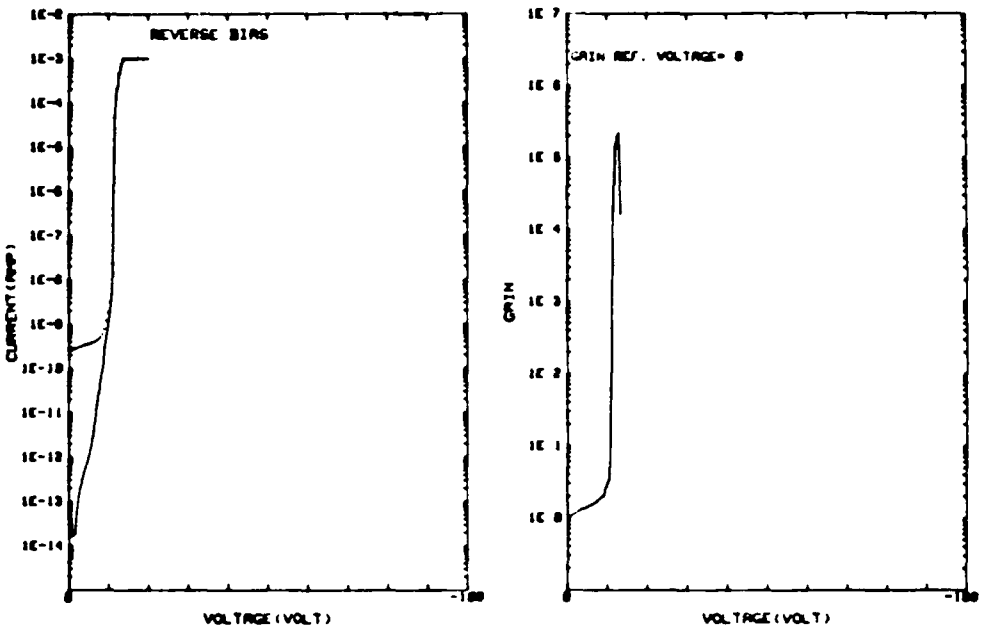

Fig. 25 (a) Light (dotted line) and dark (solid line) log I-V curves showing low breakdown typical of the $Al_{0.6}Ga_{0.4}As/GaAs$ S.L. structure grown with a (low As/Ga ratio of 20. (b) Calculated gain (photomultiplication factor) curve for the device of Fig. 7a. Note low gain at breakdown.

photon absorption among the various regions of the structures for red (0.660 μm) and green (0.560 μm) light.

For structure B40315B, the calculations indicated that the top 1.2 μm GaAs absorbed 41% of the unreflected red light and 70% of the green light. The underlying superlattice region absorbed another 18% of red and 17% of green light. An additional 5% of red light and 3% of green light was absorbed in the 0.7 μm n-GaAs buffer layer, with the remainder of both colors being absorbed in the GaAs substrate and thus making little contribution to photo current. The photomultiplication gain at 0.9 V_{BD} was typically ~ 2.0 for red illumination and ~ 3.0 for green.

Higher gains for green illumination were typical of all structures in this series. For all the other structures and for either illumination wavelength, most of the light-generated carriers were produced in the superlattice region itself. This is largely a consequence of the fairly high transparency of the 1.6 μm thick p $Al_xGa_{1-x}As$ ($0.3 \leq x \leq 0.6$) layers for light in the 0.56 to 0.66 μm wavelength range. Unfortunately, with this diffuse type of photon absorption distribution, it is not possible to attain the pure hole or electron injection conditions necessary for separate determination of electron and hole ionization rates, α and β, multiplication Me and Mh or excess noise contributions.

This growth series has served mainly to point the way toward MOCVD growth conditions which are most favorable for producing device-quality GaAs/AlGaAs structures. In particular, a growth temperature of at least 750°C, an As/Ga

ratio ~ 33, continous growth of the AlGaAs/GaAs superlattice structure and $Al_xGa_{1-x}As$ aluminum fractions in the range of 0.3 to 0.45 appear to give devices with lowest dark currents, highest breakdown voltages and best gain characteristics.

Growth of additional structures to extend the above results has not been possible to date due to an extended period (August 1984 to March 1985) of shutdown of the MOCVD laboratory for safety modifications and to continuing conflicting priorities from other programs once the MOCVD laboratory again became operational.

2.2 Plans for Phase 2

The goal for Phase 2 of this program is to develop improved low noise APD's operating in the low loss 1.3 to 1.55 μm wavelength range. The primary focus of the experimental effort in the first part of Phase 2 will be to develop the MOCVD growth technology needed to produce high quality InGaAs/InP superlattice structures. A parallel theoretical effort to develop a practical predictive superlattice device model will also be undertaken. Later in the program the developed growth technology and modeling results will be combined to produce experimental InGaAs/InP superlattice APD's for performance evaluation. The remainder of the Phase 2 effort will be aimed at improving the performance of these devices.

3.0 SUMMARY

The technical progress in Phase 1 of this two-phase program aimed at development of low noise, high sensitivity superlattice avalanche photodiodes is reported. The initial focus of the Phase 1 effort was development of metalorganic chemical vapor deposition (MOCVD) technology for the growth of high quality GaAs/AlGaAs superlattice structures. Using the developed growth technology, two series of GaAs/AlGaAs structures were evaluated with regard to dark current, breakdown voltage, and dark and illuminated gain characteristics to study effects of variations in critical growth and structural parameters. The results will be used to guide development of a predictive performance model for this class of devices during Phase 2 of the program. The model will then be applied to optimizing design of low noise, high sensitivity InGaAs/InP APD's operating in the low loss 1.0 to 1.6 μm wavelength range. Such devices will be grown by MOCVD and their performance evaluated during Phase 2 of the program.

4.0 REFERENCES

1. R. Chin, N. Holonyak, Jr., G. E. Stillman, J. Y. Tang, and K. Hess, Electron. Lett. 16, p. 467, 1980.
2. F. Capasso, W. T. Tsang, A. L. Hutchinson, and G. F. Williams, Appl. Phys. Lett. 40, p. 38, 1981.
3. P. P. Webb, R. J. McIntyre, and J. Conradi, RCA Rev. 35, p. 234, 1974.
4. L. K. Anderson and B. J. McNurty, Proc. IEEE 54, p. 1335, 1966.
5. R. B. Emmons, J. Appl. Phys. 38, p. 3075, 1967.
6. J. J. Chang, IEEE Trans. Electron. Devices ED-14, p. 139, 1967.
7. R. A. Logan and S. M. Sze, Proc. Int'l. Conf. of Phys. of Semicon., Kyoto, 1966, J. Phys. Soc. of Japan 21, Suppl., 1966.
8. G. F. Bulman, L. W. Cook, M. M. Tashima, and G. E. Stillman, Int'l Electron. Devices Meet., p. 288, 1981.
9. Y. Takanashi and Y. Horikoshi, Japan J. Appl. Phys. 18, p. 2173, 1979.
10. J. P. Gordon, R. E. Nahory, M. A. Pollack, and J. M. Worlock, Electron. Lett. 15, p. 518, 1979.
11. N. Holonyak, Jr., R. M. Kolbas, R. D. Dupuis and P. D. Dapkus, IEEE J. Quan. Electron. QE-16, p. 170, 1980.
12. H. Shichijo, R. M. Kolbas, N. Holonyak, Jr., R. D. Dupuis, P. D. Dapkus, Solid State Commun. 27, p. 1029, 1978.
13. L. W. Cook, G. E. Bulman, and G. E. Stillman, Appl. Phys. Lett. 40, p. 7, 1982.

MISSION
of
Rome Air Development Center

RADC plans and executes research, development, test and selected acquisition programs in support of Command, Control Communications and Intelligence (C^3I) activities. Technical and engineering support within areas of technical competence is provided to ESD Program Offices (POs) and other ESD elements. The principal technical mission areas are communications, electromagnetic guidance and control, surveillance of ground and aerospace objects, intelligence data collection and handling, information system technology, solid state sciences, electromagnetics and electronic reliability, maintainability and compatibility.

Printed by
United States Air Force
Hanscom AFB, Mass. 01731

END

FEB.

1988

DTIC